Nr 118, 2005

SMHI

Meteorologi

CM-SAF

Validating the Cloud Top Height product using LIDAR data

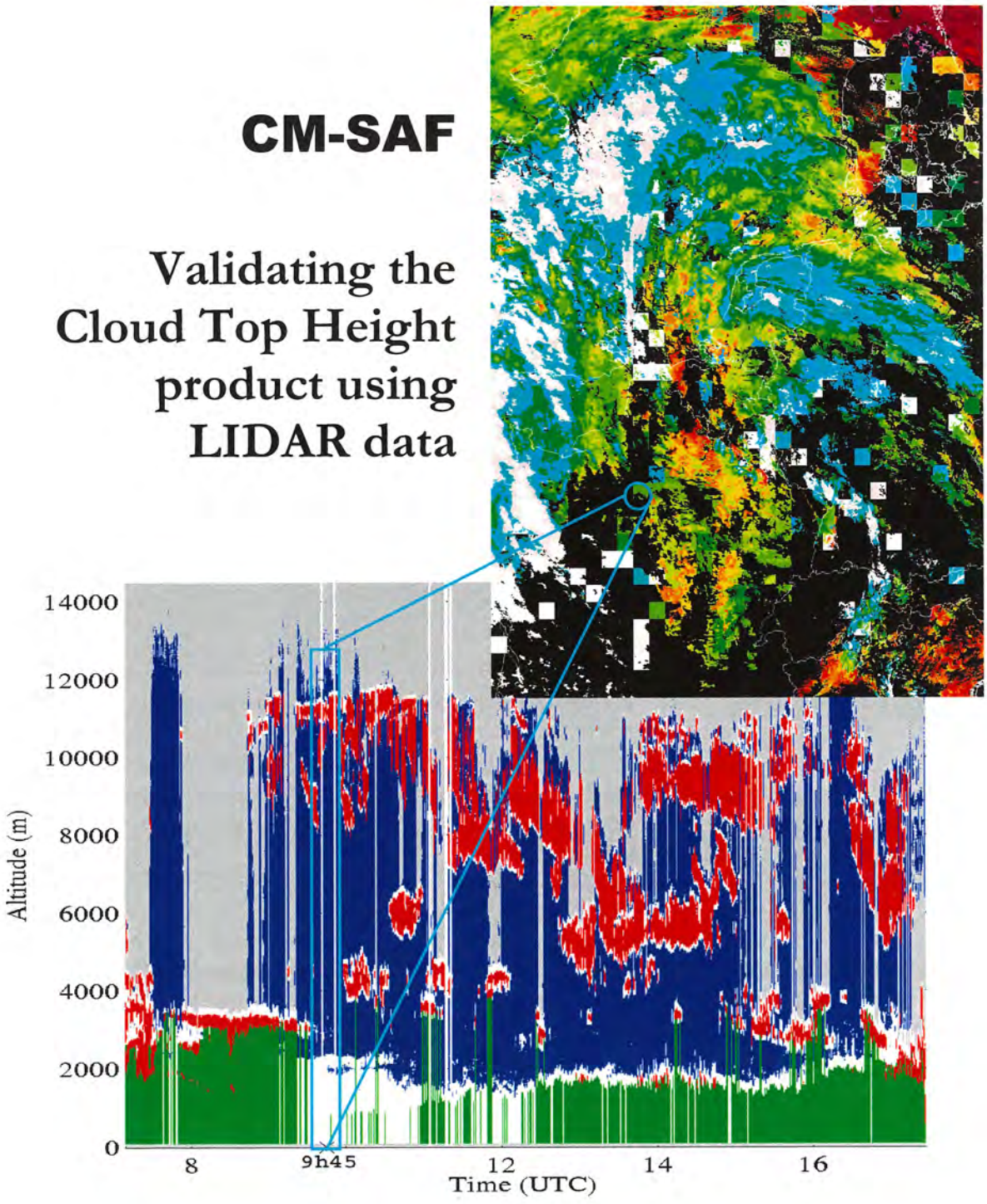

Visiting scientist report – January 2005

Matthieu Trolez, Anke Tetzlaff, Karl-Göran Karlsson

Acknowledgments

The study presented in this paper was carried out at the Swedish Meteorological and Hydrological Institute (SMHI) between August, 7th and December, 15th 2004. It was funded by EUMETSAT as part of the CM-SAF Visiting Scientist program. During this period, Matthieu Trolez was working in the Research Department of SMHI.

The authors would like to thank SIRTA (Site Instrumental de Recherche par Télédétection Atmosphérique) for providing the LIDAR data used in this study.

The people from the DWD are to be thanked for computing on demand some of the MSG data used is this study. As well, the authors are very grateful to Martial Haeffelin, from SIRTA, for transmitting the missing MSG data used for the inter-comparison.

EUMETSAT is to be thanked for permitting such studies to be carried out, thereby emulating the exchange of knowledge between scientists coming from different institutes and countries.

Matthieu Trolez would like to thank the Research Department for its hospitality and is very grateful to Anke Tetzlaff for all the time she spent helping and supporting him. Special thanks to Karl-Göran Karlsson for his hospitality and the interesting exchanges we had, to Sheldon Johnston for with help with the language and to Adam Dybbroe for his advice concerning the interpretation of the results.

Cover pictures

The cover pictures show an example of the two kinds of datasets compared in this study. The top picture represents the Cloud Top Height (CTH) above Western Europe on April, 28th 2003 at 9:45. The bottom picture shows the LIDAR data giving the structure of the atmosphere above SIRTA for the same day.
In this study, the LIDAR data is used to validate the EUMETSAT SAFNWC CTTH product. In the satellite picture, the SIRTA site is marked, while, in the LIDAR picture, the time window used for study and centred at the time of the satellite overpass is shown. The colour codes for the CTH product are given page 8 and a detailed description of the LIDAR scene is given page 16.

Abstract

This study is a validation of the SAFNWC PPS CTTH product using LIDAR data and focusing on high-level semitransparent clouds. A preliminary inter-comparison with the results of the SEVIRI algorithm is also provided.

An automated method is introduced to compare LIDAR and satellite data. It first identifies and retrieves the properties of the cloud layers in the datasets. Then, it compares their heights to the output of the CTTH product using different approaches. A case study is then performed in order to get a deeper comprehension of the results.

When comparing the highest cloud layers identified in the two datasets, a systematic underestimation of the Cloud Top Height is found. When comparing the highest cloud layer identified in the satellite data to the closest one found in the LIDAR's, a better agreement is found. This shows the inability of the AVHRR instrument to identify high-level thin cloud layers. The case study performed shows that this is especially true in case of multilayer cloud systems with a very thin cloud above a fractional opaque layer.

The inter-comparison with the SEVIRI retrievals raises difficulties due to parallax problems. This is mainly due to the large viewing angle of the SEVIRI sensor which leads a displacement further north of the high level clouds. However, the SEVIRI algorithm seems more able than the AVHRR one, to detect thin clouds as they appear thicker when seen from a slanted view.

Table of contents

1 INTRODUCTION 1

1.1 Background and objectives 1
1.2 Previous works 1

2 THEORETICAL BACKGROUND 3

2.1 LIDAR measurements 3
2.1.a The different components of a LIDAR device 4
2.1.b Capabilities and limitations of a Lidar when used for cloud detection 5
2.2 SAFNWC-CTTH products 6
2.2.a The SAFNWC PPS products 6
2.2.b The SAFNWC MSG products 9

3 DATASETS 10

3.1 LIDAR data 10
3.1.a The instrument 10
3.1.b The SIRTA STRAT algorithm 10
3.2 Satellite data: 11
3.2.a Note on the efficiency of the semi-transparent method (fraction of cases processed) 12
3.2.b Amount of data available: 12
3.2.c MSG data 12

4 METHODS 13

4.1.a Majors differences between LIDAR and satellite measurements 13
4.2 Cloud top height retrieval from LIDAR. 14
4.2.a Ideal case 15
4.2.b Real case 15
4.2.c Automated CTH retrieval using pre-processed LIDAR data: 16
4.3 Cloud top height retrieval from the satellite data 19
4.3.a AVHRR data 19
4.3.b In summary 20
4.3.c MSG data 20

5 RESULTS 21

5.1 Using dataset A 21
5.1.a The highest layer approach 21
5.1.b The closest layer approach 22
5.1.c Visual inspection of worst cases 23
5.1.d A possible explanation for the underestimation of the CTH by the semitransparent algorithm 29
5.2 Using dataset B 30
5.3 Comparison with the values retrieved by MSG-SEVIRI 32

6 CONCLUSION 35

REFERENCES 37

LIST OF ACRONYMS 39

1 Introduction

1.1 Background and objectives

Knowledge of cloud top height is important for Nowcasting and climatology applications. Satellites, by covering a large area and by giving several measurements a day, provide unique datasets that improve the reliability of forecasting and the accuracy of climatological analysis. The ability to give a reliable estimation of cloud top height from satellite-based data plays a key role in modern weather forecasting applications. The Cloud Top Temperature and Height (CTTH) product, developed within the EUMETSAT SAFNWC, aims at providing these reliable estimates. It uses data from the Advanced High Resolution Radiometer (AVHRR) onboard the NOAA polar satellites and from the Spinning Enhanced Visible and Infrared Imager (SEVIRI) onboard the METEOSAT Second Generation (MSG) satellites.

For optically thick clouds, the AVHRR CTTH retrieval is quite direct using thermal infrared data. Indeed, in this case, the radiation emitted by the atmosphere is normally very close to the black body radiation at the temperature of the atmosphere at the top of the cloud. For semi-transparent cases, radiation originating below the cloud can not be neglected. Consequently, when attempting to retrieve the cloud top height for these clouds, one has to account for this semi-transparency effect. The AVHRR CTTH product includes an algorithm developed by Korpela et al [2001] dedicated to these cases. It uses a histogram correction method based on the work of Inoue [1985] and Derrien et al. [1988].
To ensure the reliability of this product, validation studies must be carried out. Previous validations restrictively validated the CTTH product using ground based weather or cloud radar measurements. In this study, we aim to validate this product using LIDAR measurements.

The goal of this study is to validate the AVHRR CTTH retrieval for semi-transparent cases by using ground based LIDAR measurements and to find an automated way to compare satellite and LIDAR retrievals. Comparing LIDAR measurements to satellite ones is often time consuming as the LIDAR retrievals have to be visually interpreted one by one in order to extract cloud top heights. The algorithm developed in this study, retrieving heights automatically and thus allowing for automated comparison, shall be used for future validations using ground LIDAR measurements.
The main focus of this study is on the AVHRR algorithm. However, a preliminary comparison to results of the SEVIRI algorithm is also provided.

1.2 Previous works

Various studies have recently been carried out in order to validate the SAFNWC CTTH product.

Korpela et al. [2001] made a first validation using various datasets (radiosondes and ground based measurements from the CNN 1 campaign, manual reports from the Swedish air force flight missions). This study was restricted to a few cases and is therefore rather limited.

Joro et al. [2004] carried out a validation study of the SAFNWC CTTH product using weather radar data from the Finish Meteorological Institute radar network. This study focused on opaque and semi-transparent high clouds as they are more easily detected by weather radar (sensitive to large droplets or ice crystals). They reported a good agreement between the CTTH and the radar retrievals for the opaque medium and high level cloud categories as well as for the fractional/broken cloud category. For the semi-transparent high cloud category, all the comparisons were unsuccessful as the radar threshold values applied on the radar data proved to be too high. This study, by being restricted to a limited time period and emphasizing only on the high level clouds, can not be regarded as a systematic validation.

Karlsson et al. [2004] have recently performed the first systematic validation of the CTTH product, using cloud radar measurements and soundings from two major measurements campaigns (CLIWANET-CNN2 and –BBC1[1] and BBC2[2]). The re-processed radar data were visually interpreted to extract satellite data corresponding cloud top heights. They reported a good agreement between the ground-based radar and the satellites retrievals for low level clouds but a rather poor agreement for high level clouds. In case of multi-layered clouds with semi-transparent and broken clouds situations, they reported a significant underestimation of the cloud top heights.

[1] The CLIWANET was an EU founded project that aimed to provide ground observations of physical cloud parameters. Three different campaigns were held in 2000 and 2001. During the first two campaigns ground measurements were performed in 11 different sites in the BALTEX modeling area including the test sites Geesthacht, Chilbolton and Cabauw. The third campaign (BBC1) concentrated on the Cabauw site where a large number of different instruments were used to provide an extensive number of different datasets at one test site.

[2] The BBC2 campaign is a follow up project of the BBC1 campaign held by KNMI and the University of Bonn in May 2003. The main objectives of this study were similar to the BBC1 campaign. [Karlsson et al. 2004]

2 Theoretical background

2.1 LIDAR measurements

A LIDAR (LIght Detection And Ranging) is an active remote sensing device. It emits light that, while travelling trough the medium (atmosphere), interferes with the target (scatter).The backscattered light is then measured (figure 2.1). The LIDAR is a commonly used device to study different aspects of the atmosphere and of its components.

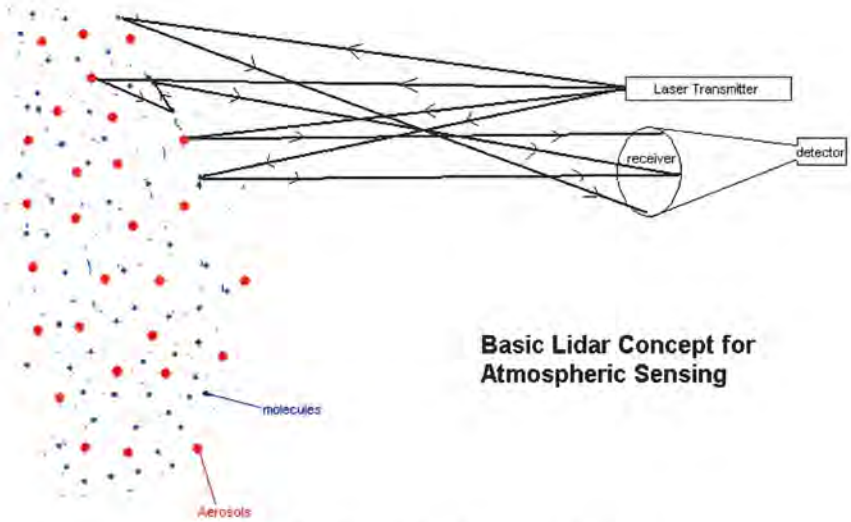

Figure 2-1 Principle of a LIDAR device[1]

Different types of physical processes in the atmosphere are related to different kind of light scattering. Optical interactions used in laser remote sensing include: Mie, Rayleigh and Raman[2] scattering, fluorescence and absorption. They allow, from the measurement of the backscattered light, to gather various information including the distance of the target, its velocity or its chemical composition.

Several types of LIDAR are associated with these different scatterings:

- Backscattered LIDARs measure the backscattered radiation at a defined wavelength chosen according to the selected target. For example, they can be used to measure aerosols concentration.
- Doppler LIDARs measure the Doppler shift between the emitted and the backscattered radiation, allowing for wind speed measurement for example.
- DIALs (Differential Absorption LIDARs) operate at two different wavelengths. By comparing the difference between the two absorption coefficients chemical species concentrations of the target can be retrieved.
- Raman LIDARS can measure gaseous species (O_2, N_2 or H_2O) by measuring the Raman shift in the backscattered radiation (e.g. pollutants in a smokestack's plume).

[1] source www.ece.arizona.edu/ ~arsl/LIDAR.html

[2] Raman scattering is an inelastic scattering which induces a shift in the frequency of the backscattered photons. This shift is due to the energy absorbed (or released) by the scattered molecule.

2.1.a The different components of a LIDAR device

The emitter

In a LIDAR, light is emitted by a laser device at a selected frequency in the ultraviolet, visible or infrared regions. A laser is used for the properties of its light: collimated, monochromatic and coherent. The light outputted can have its frequency doubled, tripled or quadrupled

Examples of commonly used lasers:

- Tripled or quadrupled Hd:Yag lasers or rare-gas halogen lasers (KrF, XeCl or XeF) for LIDARS working in the UV region
- Alexandrite and Ti:sapphire lasers for the near infrared
- CO_2 lasers for the far infrared.

In most lidars, the light emission is pulsed and the travel time of each pulse measured. It is the time difference between the emission and the reception of a pulse. Using *equation 1* the distance r between the device and the target can then be deduced.

$$2 \cdot r = \tau / c \qquad \textit{(equation 1)}$$

with τ the time between the emission and the reception of a given pulse and c the speed of light. A small fraction of the output is often sampled to provide a zero time marker and to check the wavelength.

The receiver

The backscattered photons are collected by means of one or several optical telescopes coaxial to the laser beam. These telescopes are chosen by considering the overlap between their field of view and the location of the targets. For example, in a single lidar device, the lower part of the tropopause can be studied using a large field of view telescope while the higher parts are studied with a narrow field of view one.

The detector and the output

To measure the intensity of the backscattered signal, the photons received by the telescopes are filtered and counted. During the filtering, only photons at wavelength of observation are kept. To achieve this, spectral analysers are used to discriminate against radiation at other wavelength. The counting of the remaining photons is performed by photo-detectors. In the 200-900nm region (ultraviolet to near infrared), photomultipliers are preferred for their low noise and high gain. Photo-diodes are more commonly used in the infrared region and often as avalanche photodiodes (because of their inherent internal gain).

As the emission is pulsed, the information is time sampled. When analysing the atmosphere, each time sample is a vertical profile of atmospheric properties. Figure 2.2 shows an example of LIDAR measurement. In each profile, the intensity of the backscattered signal as a function of the altitude is measured. These profiles can be averaged (for example on a 10 seconds basis) to reduce the data size.

A more detailed description of LIDAR remote sensing, including a description of the general principles as well as a description of different LIDAR devices, is given by Raymond Measures [1992].

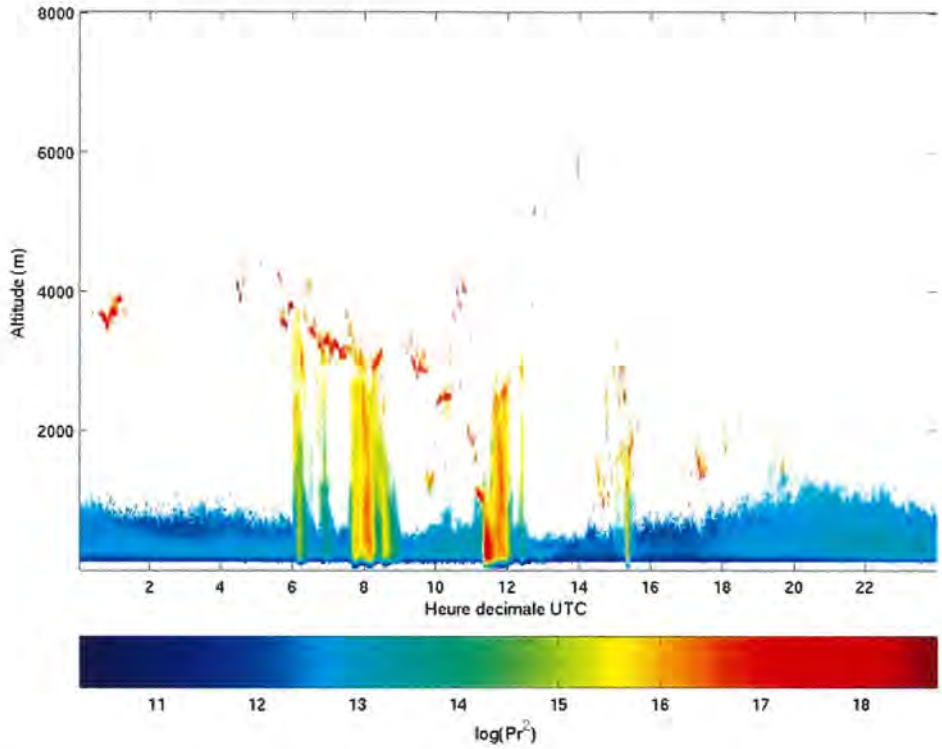

Figure 2-2 example of backscattered LIDAR profiles. The amount of power return is given as a function of time and altitude (07 July 04, SIRTA station)

2.1.b Capabilities and limitations of a Lidar when used for cloud detection

Cloud remote sensing is often perfomed using Radars and LIDAR instruments. Below is a comparative presentation of their characteristics.

Radars

Ground based cloud observations are often performed using cloud or weather radar devices:

- Weather radars benefit a well developed network. They are mainly limited by the radar sensitivity which only allows for cloud detection close to the radar site, the radiation dispersion which distributes the transmitted power in more than one direction, the side lobe contribution which contaminates the received signal and the probability for cloud top overshooting.

- Cloud radars usually operate at higher microwave frequencies to detect small cloud droplets. The attenuation in clear sky being relatively strong at high frequencies, a cloud radar device typically points vertically. As water droplets absorb these frequencies, cloud radar devices are limited to fair weather conditions without deep absorbing clouds or precipitation. It is a very precise but expensive instrument making it quite rare [Joro et al. 2004].

LIDARs

The primary advantage of using a LIDAR system over both weather and cloud radars is its higher sensitivity and spatial resolution due to the shorter wavelength used. Indeed, an object can generally be detected by the mean of an electromagnetic wave when its size is at

least as big as the wavelength. As a consequence, LIDAR systems, which have a wavelength in the visible spectrum ($3x10^{-7}$ *to* 10^{-6} *m)* offer a resolution thousands of times greater than radar systems (with wavelength around *1 cm*). The operating wavelength of a LIDAR device is so small that LIDAR are often used for measurements of smoke, aerosols or even air molecules.

Another advantage of LIDAR against radar devices for atmospheric analysis lies in the strong interactions that many chemical substances have at short wavelengths. This allows for remote mapping of atmospheric contents by the use of suitable combinations of lasers and by looking for changes in the spectrum of the return signal (Dial and Raman LIDARS).

The major limitation when using a LIDAR for cloud detection lies in the high sensitivity of the device to the opacity of the atmosphere. When the laser beam passes through a highly opaque zone (e.g. water cloud), most of its photons are scattered, leading to a high backscattered signal but also to a high loss in the power of the vertically propagating beam. As a consequence, the LIDAR can hardly detect the top of water clouds and the signal above them is lost (no power is returned). However, this limitation affects mainly the opaque cloud cases but won't prevent a good retrieval of cloud tops in semi-transparent cases.

2.2 SAFNWC-CTTH products

The EUMETSAT SAFNWC Cloud Top Temperature and Height Products (CTTH) provide Cloud Top Height (CTH) and Cloud Top Temperature (CTT) estimates derived from satellite data. The CTTH retrieval mainly aims at Nowcasting applications, e.g. early warning of thunderstorm development and height assignment for aviation forecasting. In addition, the CTTH product is used to build up cloud climatologies within the CM-SAF.

2.2.a The SAFNWC PPS products

The SAFNWC Polar Platform System (PPS) products are based on NOAA AVHRR satellite data. The PPS cloud scheme includes two different CTTH retrieval methods according to the type of clouds: one for opaque clouds and one for fractional and semi-transparent clouds.
In case of opaque clouds, the brightness temperatures from the AVHRR IR channel are used in combination with NWP datasets to calculate the cloud pixel corresponding CTTH values. In case of semi-transparent and fractional clouds, a histogram technique is used that aims to compensate for the contribution of ground radiances in the investigated pixel. A short description of the two algorithms is given below. Additional details can be found in the scientific user manual for the AVHRR SAFNWC products [Thoss and Dybbroe, 2004].

Opaque CTTH retrieval

For pixels classified as opaque clouds, the Cloud Top Pressure (CTP) is derived from a best fit comparison between the simulated and measured brightness temperatures of channel 4. The simulated cloud free and cloudy TOA radiances (resulting when inserting a black body radiating cloud layer at various vertical atmospheric levels) and temperatures are calculated for the AVHRR Thermal Infrared channels applying the RTTOV radiative transfer model [Eyre 1991] and using temperature and humidity profiles from NWP data. From the computed pressure, the CTH and the CTT are retrieved.

Semi-transparent and fractional CTTH retrieval

For all pixels classified as semi-transparent or fractional clouds, the cloud top temperature is derived using a histogram technique based on the work of Derrien et al [1988] and Inoue

[1985]. The method uses the brightness temperatures of AVHRR channel 4 and 5 (T_4 and T_5). It is based on the often observed arc-like structure of the two-dimensional histograms T_4-T_5 versus T_4 over regions of semi-transparent or broken clouds.
This distribution can be explained theoretically when making a few simple assumptions:

- no atmospheric absorption, local thermodynamic equilibrium
- constant absorption coefficient throughout the cloud layer
- brightness temperature depending nearly linearly on radiance (true for long wave infrared frequencies)

From this theoretical shape and the observed distribution, a minimization method (Levenberg-Marquardt least square fitting method) is used to find the most likely parameter values. More on the method and its implementation can be found in Korpela et al. [2001]. Due to the fact that the histogram method has to be applied to a group of image pixels rather than to single pixels, the semi-transparent cases are grouped into squares (32x32 pixels wide) and only one CTTH value is assigned for the entire square of pixels.

The final CTTH output includes, beside cloud top height in pressure units, cloud top temperature and cloud top height in meters for both opaque and semi-transparent cases. An example of the CTTH output is visualized in figure 2.3. It is important to note in figure the squared CTTH values which result from the semi-transparent retrieval method. In addition, figure 2.3 illustrates that not all clouds have a corresponding CTTH value due to a non-convergence of the semi-transparent correction method.
Beside the CTTH product, several cloud and precipitation products are derived from AVHRR data using the SAFNWC PPS. For this validation study we have used the following SAFNWC products in addition to the CTTH retrieval:

Cloud Mask (CM)

The CM seeks to identify all absolutely cloud free pixels in a satellite scene. The algorithm is based on a multi-spectral threshold technique applied to each pixel of the satellite scene. The threshold tests are coupled, or grouped together, so that the identification of a cloud free or cloud contaminated pixel requires that several threshold tests must be passed. The thresholds used are dynamic and take into account the current atmospheric state, the actual illumination, viewing conditions and the state of the surface within the satellite footprint. They are derived by calculating the cloud free satellite signal using RTM simulations. More on the derivation of dynamic thresholds can be found in Dybbroe et al. [2005a]. In addition to these dynamics thresholds constant or linearly varying thresholds, determined empirically, are applied [Dybbroe et al., 2005b]. Finally a filtering is applied on the pixels classified only using AVHRR channel 3B in order to correct artificial results due to channel 3B noise. The cloud mask is used as an input for the Cloud Type product.

Cloud Type (CT)

The CT aims to provide a detailed cloud scene analysis which distinguishes between generic cloud classes (fractional clouds, semi-transparent clouds, high, medium and low clouds). The CT algorithm is a multi-spectral threshold retrieval applied to each pixel of the satellite scene. It employs a sequence of threshold tests in an *if-then-if* structure and stops if a threshold test is successful. Contrary to the CM algorithm, the threshold tests in the CT algorithm often use few or even a single feature. During the daytime, the sequence of tests produces cloud categories in the following order: fractional water clouds, thin cirrus, fractional ice clouds, and opaque clouds. During night and twilight conditions, the first

category is removed. The Cloud Type product is used as an input for the CTTH product. Figure 2.3 gives an example of the CT product output.

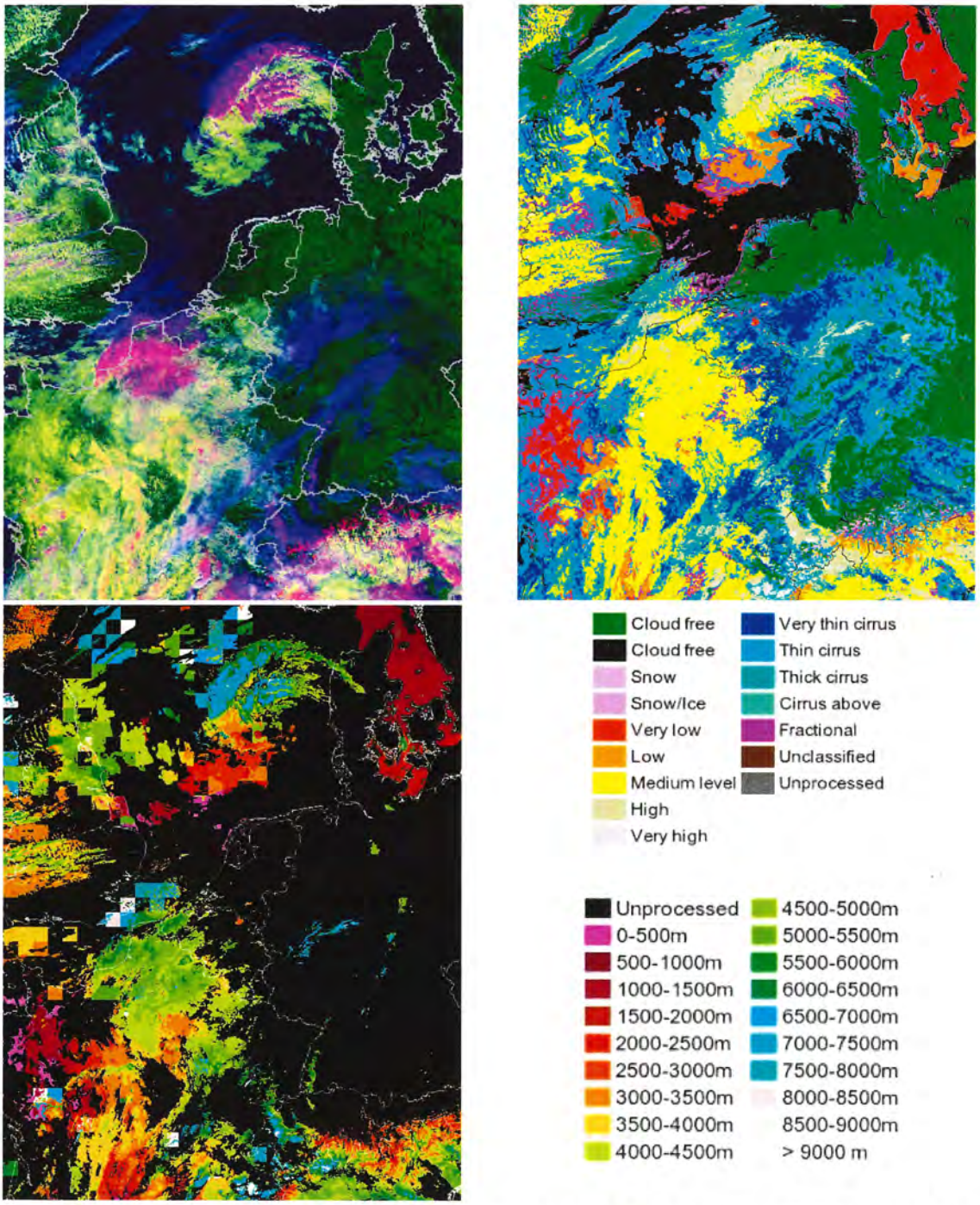

Figure 2-3: Composite image of channels 1, 3 and 4 (top left), CT (top right) and CTTH products and colour codes for a NOAA scene, 20th April, 2003, 12h47 UTC over north-western Europe (CNN-II area). One can note the large squares in the CTTH product corresponding to the area used to perform the histogram method for semi-transparent clouds. Black squares indicate that no value was found even if some semi-transparent clouds were identified (e.g. in the top left part of the CTTH pictures).

2.2.b The SAFNWC MSG products

The SAFNWC Meteosat Second Generation (MSG) products are based on MSG SEVIRI satellite data. Different retrieval techniques are used, depending on the type of clouds and on the availability of the SEVIRI and NWP data.
A short description of the general CTTH retrieval process[1] is given below. More information can be found in the scientific part of the user manual provided by the SAFNWC /MSG [Le Gléau, 2004].

CTTH retrieval process

- RTTOV [Eyre et al. 1991] is applied using NWP temperature and humidity vertical profiles to simulate cloud free and overcast radiances and brightness temperatures for each SEVIRI channel.
- For low, medium or high opaque clouds, the CTP is retrieved using an identical method to the one used for the opaque clouds in the AVHRR scheme. In this method, a best fit comparison between the measured and the RTTOV simulated 10.8μm brightness temperatures is performed.
- For high semitransparent clouds, a correction for the semi-transparency is applied. The CTH is retrieved from the study of pairs of infrared channels: one window channel and one sounding channel[2]. The idea behind this use is that the effect of clouds is different in a window channel than in a sounding channel.

Different methods are successively tried to retrieve the semitransparent CTP:

- First, the H_2O/IRW method [Schmetz et al. 1993] is applied. This method is based on a bi-dimensional (window and sounding radiances) histogram analysis. It is successively applied to the different sounding channels (13.4, 7.3 and 6.2μm) and the final result is the average value of the different cloud top pressure thereby retrieved.
- Then, if no result could be obtained with the H_2O/IRW intercept method, the radiance ratioing method [Menzel et al. 1982] is applied to the 10.8μm and 7.3μm radiances. This method allows retrieval of opaque cloud radiances, from measurements made in two different channels through a direct relation between, the radiance quotient and the atmospheric pressure. If no result can be obtained, the method is applied to the 6.2μm and finally 13.4μm radiances.
- If the radiance ratioing technique leads to cloud top temperatures warmer than the corresponding 10.8μm brightness temperatures, the method for thick clouds is used instead.

- CTH and CTT are then computed using general modules.

[1] used when all mandatory data is available
[2] In a window channel the atmosphere is transparent. Consequently, measurements made in a window channel include contributions from the whole atmosphere down to the ground. On the contrary, in a sounding channel the atmosphere is more or less opaque. Because of this opacity, higher layers contribute more to measured radiances than lower ones.

3 Datasets

3.1 LIDAR data

The data used in this study was provided by Site Instrumental de Recherche par Télédédection Atmosphérique (SIRTA), located on the campus of Ecole Polytechnique, Palaiseau, France with geographical coordinates: *48.7 N – 2.2 E.* The LIDAR datasets used for the validation study are preprocessed datasets. They are the output of the STRAT (Structure of the atmosphere) algorithm developed at SIRTA.
The following sub-sections include a short description of the SIRTA STRAT algorithm as well as a short description of the SIRTA LIDAR device. More information on SIRTA can be found on the SIRTA website[1] and in Haeffelin et al. [2005].

3.1.a The instrument

The LIDAR instrument used is a backscattered LIDAR (see section 2.1 for a description of the different kinds of LIDAR) so-called LIDAR Nuages Aérosols (LNA) dedicated to the study of clouds and aerosols. It can detect aerosols and cloud layers with visible optical thickness ranging from 0.05 to 3.

The LNA is a Nd-Yag pulsed LIDAR emitting at 532 and 1064 nm and linearly polarized. Backscattered photons are collected through two telescopes: a narrow-field-of-view one (0.5 mrad) with range 2-20 km and a wide-field-of-view one (5 mrad) with range 0.1-5 km. Both have a vertical resolution of 15m.

The LNA is manually operated. Profiles are generally collected from Monday to Friday, 08:30 to 19:30 local time. Measurements are occasionally performed earlier in the morning[2]. However, as the LIDAR is turned off when precipitations occur, no continuous series of data were really available for the study. Consequently a significant portion of the satellite scenes available could not be used.

3.1.b The SIRTA STRAT algorithm

Raw LIDAR data gives the amount of backscattered photons as a function of altitude for every profile, providing information on the optical density of the target (see Figure 2-2). The product used in this study is the output of the STRAT algorithm (beta version). This algorithm, applied on the raw LIDAR data, identifies the different layers crossed by the laser beam. In the beta version, each pixel can be classified as:

- **No significant power return (NSPR)**: the backscattered signal is considered too noisy for identification. A signal is considered too noisy when the signal to noise ratio is smaller than 3. The noise is caused by optical and electronic variations and is considered constant along the profile. It is estimated by taking the standard deviation of the signal where there is no LIDAR return in the highest range i.e. where the signal is totally due to sky

[1] http://sirta.lmd.polytechnique.fr
[2] Many measurements used were actually performed between 06:00 and 08:30.

radiance. The NSPR flag is present when the LIDAR beam has been too much attenuated by the atmosphere.

- **Boundary layer:** the pixel is part of the boundary layer. The boundary layer is the lowest layer of the atmosphere in contact with the ground. It is typically between 1000 and 2000 meters thick, depending on the intensity of the turbulent mixing (normally lower during night than during day). In this layer, where turbulence induced by the ground is very strong, the dynamics are different than in the higher layers (part of the free atmosphere). Most of the aerosols from the ground, mixed by turbulent flow, are found inside this layer. In the STRAT algorithm (beta version), the boundary layer identification is from a threshold test performed on the ratio of the backscattered signal between two heights.
- **Molecular:** the atmosphere is cloud and aerosol free. In the STRAT algorithm (beta version), a molecular backscattering profile is estimated from pressure and temperature profiles (measured by daily atmospheric sounding or extracted from models) and then compared to the actual backscattered signal. Molecular layers correspond to zones that successfully passed a threshold test relevant of the similarity between the slopes of the simulated and of the measured profiles.
- **Cloud or aerosol:** Cloud or aerosol is present at the corresponding location of the pixel. In the STRAT algorithm, Continuous Wavelet Transform [Mallat et al. 1992] is used to detect singularities of the LIDAR signal at cloud top, peak and base. A threshold test is then used to remove over detections due to noise variations.

A complete description of the STRAT algorithm can be found in Morille et al. [2004]. Before reading the referenced article, please note that the version of the algorithm described in there is an upgrade of the version used for this study. We used the beta version of the algorithm that does not make the distinction between clouds and aerosols. In the upgraded version, a new module, making this distinction, was added. Apart from this module, the description given corresponds to the beta version.

3.2 Satellite data:

Satellite PPS measurements were performed by NOAA-15, 16[1] and 17 satellites. Each of these satellites provides two measurements a day over the region of study. The AVHRR data was collected at SMHI over two different periods:

- **March and April 2003**. The data was available as it had been used for preceding validations (Karlsson et al. [2004]).
- **March to July 2004**. The data had been systematically collected for this study.

Both periods were used in order to maximise the number of cases available.

A total of 211 AVHRR scenes covering the SIRTA test-site were processed to compare satellite PPS derived CTTH products with ground based LIDAR datasets. The processing of the AVHRR level 1b data was performed using the SAFNWC ACPG software version 1.0 using HIRLAM analysis datasets as ancillary NWP input. Different levels of processed data were used in this study:

- Remapped AVHRR radiance images were used for the visual inspection of selected cases.

[1] A problem with the AVHRR instrument onboard NOAA 16 causes the sensor to sometime jitter, leading to a noisy pattern (zigzag shape) in some pictures. Consequently, some scenes had to be excluded after a visual inspection.

- The SAFNWC CTY product was used to identify the cloud type of the investigated satellite PPS datasets.
- The SAFNWC CTTH product was used to carry out the comparison with retrieved LIDAR heights.

3.2.a Note on the efficiency of the semi-transparent method (fraction of cases processed)

In order to validate the semi transparent retrieval method, it is important to estimate the fraction of semi transparent cases actually processed. Indeed, as the method is based on the fitting of the data to a theoretical curve, some cases don't give any valid result as no convergence is found. To estimate the fraction of cases actually processed, the study is carried out on a set of 211 satellite PPS scenes. Inside a square box surrounding the SIRTA site (9x9km wide), the cases classified as semi transparent or fractional clouds by the Cloud Type are selected. In this selection, the number of pixels with a valid CTTH retrieval is counted. Following this method, 1255 out of 4666 pixels have a valid semi-transparent retrieval. Consequently, the CTTH retrieval method for semi-transparent clouds gives a valid result in only about 27% of the cases.

3.2.b Amount of data available:

From the 211 NOAA scenes processed for the whole period of study[1], 198 were corresponding to a simultaneous LIDAR measurement. Out of these, 166 scenes had cloud layers identified in the LIDAR data. Finally, 92 scenes were considered to be sufficiently cloud filled for this validation, i.e. the CTTH data available in a square box (9x9 km wide) around the test site was higher than 50%.

3.2.c MSG data

The MSG data used for the inter-comparison between the two different satellite retrievals was collected once the final list of NOAA AVHRR scenes had been established.
Once the dataset was split (see part 4: Major differences between LIDAR and satellite measurements), 34 MSG scenes were available for comparison on high level clouds. The missing scenes are mainly due to the unavailability of the data for the year 2003. Out of these 34 scenes, 30 scenes were considered sufficiently cloud filled for comparison.

[1] Only the scenes of the LIDAR's operating days were processed.

4 Methods

4.1.a Majors differences between LIDAR and satellite measurements

LIDAR and polar satellite data are very different kind of data; we will mention two major differences that affect our study.

First, the LIDAR instrument retrieves atmospheric properties at a fix location and for a certain time period while the satellite gives a general picture of the area at a fix time (acquisition time). Consequently, LIDAR measurements correspond to a single point in the satellite picture while, symmetrically, satellite measurements correspond only to one LIDAR profile made at the precise acquisition time.
Different factors lead to uncertainty in the comparison:

- The satellite resolution (approximately one square kilometre for the AVHRR instrument) is far bigger than the section of the LIDAR beam (a few square metres, depending on the altitude[1]). Consequently, the satellite measurement is actually the average over a spatial box of the cloud top heights a LIDAR would retrieve. In addition, the remapped AVHRR datasets still can have a significant geometric dislocation. The Accurate Navigation of AVHRR (ANA), based on the utilisation of known landmarks, is used to limit this dislocation. Finally, the maximum dislocation error is normally smaller than 4 kilometres and is generally below 2 kilometres [Brunel et al, 2000].
- The information available for the acquisition time, in the filename of the SAFNWC PPS products, corresponds to the time of the satellite overpass over the region. It is not precisely the overpass time at the LIDAR ground station. There is thus imprecision on the acquisition time above the LIDAR site.

To overcome these uncertainties, the data was averaged both in time (LIDAR data) and space (satellite data). Therefore, in this study LIDAR values averaged over a time window are compared to satellite values averaged over a space window. It is important to note that the sizes of these windows are related: the larger the time window, the larger the space one. For this study, a space window of 9 by 9 kilometres and a time window of 30 minutes are used. This follows from the results of Wolters et al.[2] who studied the effects of various spatial and time window sizes for AVHRR radar based validation studies.

The second major difference between satellite and LIDAR acquisitions is due to the fact that the LIDAR we use is ground based. The higher the LIDAR beam penetrates the atmosphere the more it is attenuated. Moreover, as water clouds can even stop the beam completely, a high fraction of low level clouds prevents any retrieval from higher layers. It induces a high uncertainty in the cloud top measurement (the beam can be stopped inside the cloud). On the contrary, as a satellite is viewing the atmosphere from above it is restricted to see only the uppermost cloud layers.
This difference is crucial and can lead to a high uncertainty in the comparison. Indeed, to compare cloud top heights, one has to ensure that both devices observe the same cloud layer.

A first approach is based on the use of the NSPR flag[3] that indicates when the signal is too attenuated to be significant. The height of the highest level with significant power return is identified by the STRAT algorithm and is compared to the height of the layer retrieved by

[1] Although the beam is almost parallel, it does diverge a small amount. A typical value for the divergence angle is 0.5mrad, leading to a beam diameter of 0.5m at 1km altitude and 5m at 10km.
[2] Personal communication
[3] No Significant Power Return, see part III.1, description of the STRAT output

the PPS CTTH product. If the LIDAR maximum height is lower than the AVHRR-derived height, the case is excluded. This filtering aims to ensure that a LIDAR measurement is performed at the height of the selected AVHRR layer. However, because the information can be ambiguous in the case of broken low level water cloud, it is not sufficient. A stronger filtering on the LIDAR data has therefore to be applied

To identify the cases were low level water clouds are likely to have disturbed the LIDAR measurement, we distinguish between two kinds of LIDAR retrievals: the ones with retrieval above 4000m and the ones without. Assuming that most of the clouds above this height are ice clouds -which, in most cases, are not capable of completely stopping the beam- and that most of the water clouds -which often stop the beam- are found under this height, this distinction splits the dataset in two parts: very reliable and less reliable.

- **Dataset A:** Cases with retrieval above 4000m (44 cases).
- **Dataset B:** Cases with no retrieval above 4000m (48 cases).

Dataset A, used mainly to study high level clouds, is thought to exclude most of the cases where low level water clouds dominates within the 30 minutes time window. Even if it also includes some cases with low level water clouds and even a few cases of high level water clouds, these contain holes or are thin enough to allow for a retrieval of the upper layers. This dataset is believed to be very reliable since the LIDAR retrieval can here range up to the upper part of the atmosphere.
Dataset B is expected to contain cases where low level water clouds dominate within the investigated time window. These LIDAR retrievals are considered to be less reliable dataset A as no information is available on the state of the atmosphere above the low level cloud layers. Moreover, the retrieval of the cloud top height can often be underestimated as the LIDAR beam might have been stopped before reaching the top of the cloud. This dataset is then used to try to validate the CTTH product for low level clouds and especially broken low level clouds.

4.2 Cloud top height retrieval from LIDAR.

In order to compare CTTH retrievals from LIDAR and satellite in an effective way, an algorithm, that identifies the different cloud layers in a LIDAR dataset and retrieves their average top height, was developed. In addition, secondary information, including for example the average cloud base height, the length of the layer and information about the range of the LIDAR for each measurement, was retrieved. This secondary information is used to estimate the quality of the height retrieval and the actual situation.

The LIDAR data used is the output of the LIDAR cloud mask described in section III.1. This product is very useful for our study, as it allows us to focus on the identification of cloud layers and on their boundaries (top and base height).

Within a time window, this data can be seen as a two dimensional array of flags with the following properties:

- A column represents a vertical profile (one profile being 30 seconds long).
- A horizontal line represents a defined altitude (one raw every 15 meters).
- The flag can be set to one of the following values: 0 (no significant power return), 1 (molecular scattering), 2 (boundary layer), 3 (cloud or aerosol) or 10 (undefined). See section 3.1, description of The SIRTA STRAT algorithm, for details.

4.2.a Ideal case

In an ideal situation (no noise in the data) and according to the preceding description of the datasets, a cloud can be defined as a contiguous group of pixels identified as cloud filled (flag 3) surrounded by pixels identified as molecular (flag 1). The detection of cloud properties then consists in taking the average of the height values of the highest (and lowest) pixel included in the selected cloud. The cloud's length is the number of columns on which the group is spread. Refer to Figure 4-1.

1	0	1	0	0	0	1	0	1	0	1	0	1
1	1	1	1	1	1	1	1	1	1	1	1	1
1	1	1	1	3	3	1	3	1	1	1	1	1
1	1	3	3	3	3	3	3	3	3	3	1	1
1	1	1	3	3	3	3	3	3	3	3	3	1
1	1	1	1	1	3	3	3	3	3	1	1	1
1	1	1	3	3	3	3	3	1	1	1	1	1
1	1	1	1	3	1	3	1	1	1	1	1	1
1	1	1	1	1	1	1	1	1	1	1	1	1

Figure 4-1 : Example array representing a cloud in an ideal situation, the LIDAR beam reaching the atmosphere above the cloud.

In this ideal situation, when a cloud is optically too thick for the LIDAR to fully penetrate it, the situation is the same as above, with the only difference being that above the cloud the flag is set to 0. Refer to Figure 4-2.

1	1	0	0	0	0	0	0	0	0	0	0	1
1	1	1	0	0	0	0	0	0	0	0	0	1
1	1	1	0	0	0	0	0	0	0	0	0	1
1	1	3	0	0	0	0	0	0	0	3	1	1
1	1	1	3	3	3	0	3	3	3	3	3	1
1	1	1	1	1	3	3	3	3	3	1	1	1
1	1	1	3	3	3	3	3	1	1	1	1	1
1	1	1	1	3	1	3	1	1	1	1	1	1
1	1	1	1	1	1	1	1	1	1	1	1	1

Figure 4-2 : Example array depicting a thick cloud in an ideal situation, the LIDAR beam being stopped inside the cloud.

4.2.b Real case

The situation described above is unfortunately not relevant of the real data analyzed. Figure 4-3 gives an example of the data actually processed. The major differences are:

- The STRAT algorithm has difficulties in identifying a molecular sky when a cloud is too close. Consequently the clouds are often surrounded by this undefined flag (10).
- Because of measurement noise, the result of the cloud mask includes noise as well. This noise consists in the presence of cells with value 10 (undefined) ("holes") inside a group of cloudy ones.

- In case of multi-layer situations, if the bottom layer is fractional or with an optical thickness close to the maximum value for LIDAR penetration, the highest layer can only be partially identified.

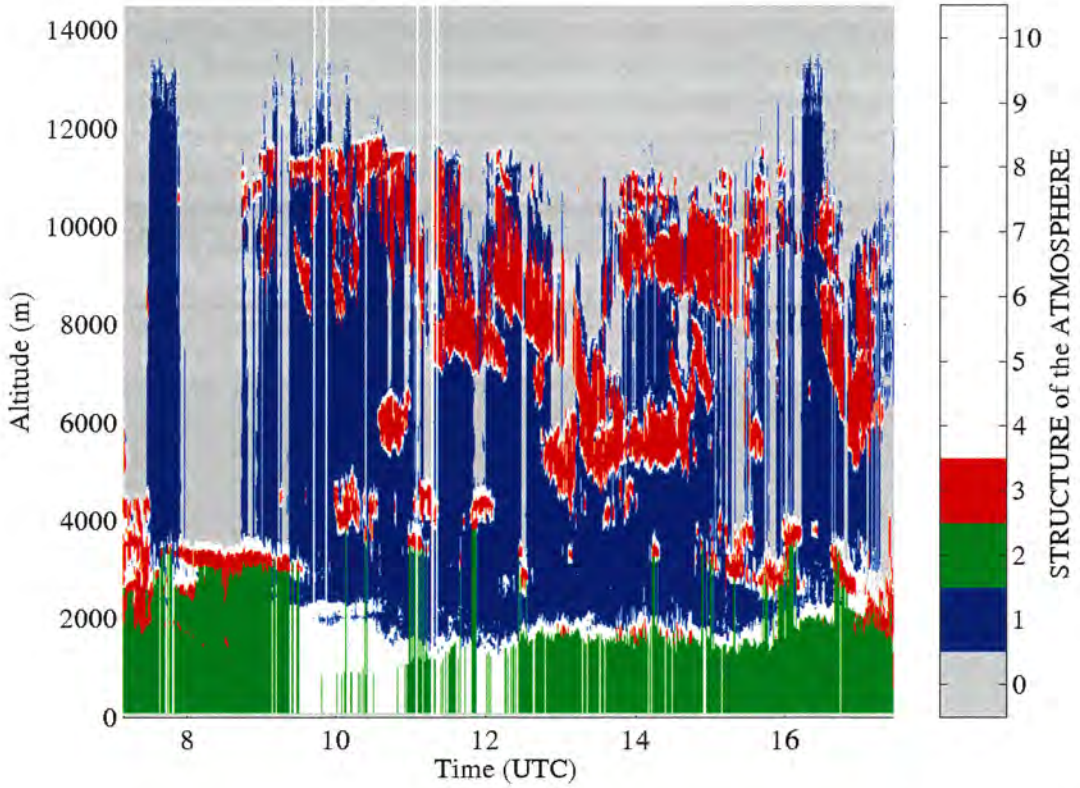

Figure 4-3: Example of a multi-layer situation (28 April 03) illustrating the complexity of the actual dataset. (1): A lower cloud layer prevents any retrieval of the atmosphere above it (between 7:00 and 9:30). (2): Because of underlying clouds, the detection of the upper layers is often only partial (e.g. close to 9:00 and 16:00). (4) An identified cloud is often surrounded by the undefined flag. (5) Some holes are included inside an identified cloud (e.g. at 8:00). See Figure 5-3 for colour code.

4.2.c Automated CTH retrieval using pre-processed LIDAR data:

When performing a visual inspection of the LIDAR data, the above mentioned problems can be overcome quite easily by interpreting and extrapolating. The "holes" in a cloud are interpreted either as noise in the detection or as a separation between layers. The continuity of a layer is extrapolated when its detection is only partial.
Considering an automatic approach a way to define clouds has to be found. According to this definition, the algorithm is requested to:

- Identify the different cloud layers (even if surrounded by undefined values).
- Overcome the problem of "holes" in the data.
- Retrieve each layer's properties even if its detection is only partial.

As this identification is to be performed over a relatively small time window (typically 30 minutes), it is assumed that there exists a cloud free level between two different cloud layers (i.e. the lowest part of a higher layer is above the highest part of a lower layer).
Under this assumption a cloud layer is defined as a group of cloudy pixels continuous in altitude.

The flowchart of the algorithm is given in figure 4.4. The automated CTH retrieval is performed using an iterative approach.

The input for the algorithm is the STRAT product for the time window centred on the satellite overpass (or acquisition) time.

Module I
A list of all the cloudy segments in the data is created by identifying them in each profile. A cloudy segment is defined as a vertical contiguous group of pixels with value 3.

In modules 2 to 5, the list of cloudy segments output by module I is classified into different cloud layers, using an iterative approach performed over the whole dataset.

Module II
A new layer is first created by selecting a cloudy segment not yet classified. Its vertical limits (bottom and top) are retrieved. The new layer is then defined as a group of adjacent pixels in the horizontal (i.e. in the neighbouring profiles).

Module III
The layer is completed by adding every cloudy segment that is partly inside its limits. The new limits of the layer are retrieved, taking into account its new elements. These limits are the top of the highest segment of the layer, and the bottom of the lowest one.

Module IV
The new limits are compared to the ones found before the last completion (i.e. previous iteration of module III or module II if first iteration). If they are different the next step is module III (new iteration), if they are equal the next step is module V (layer complete).

Module V
The list of cloudy segments is searched for an element not yet classified. If one is found the next step is module II else it is module VI.

Module VI
The properties of each layer are retrieved. They are: the average top and bottom heights, the average height of the highest significant retrieval above the layer, the length (number of profiles times 30 seconds) of the layer.
-**Module VII**: A filtering is applied according to the length of the layer to ensure the significance of the dataset. A layer has to last more than 5 minutes to be kept for comparison.

The output of this retrieval is a list of the different cloud layers identified in the time window, detailing their vertical boundaries, their length and the range of the LIDAR measurement.

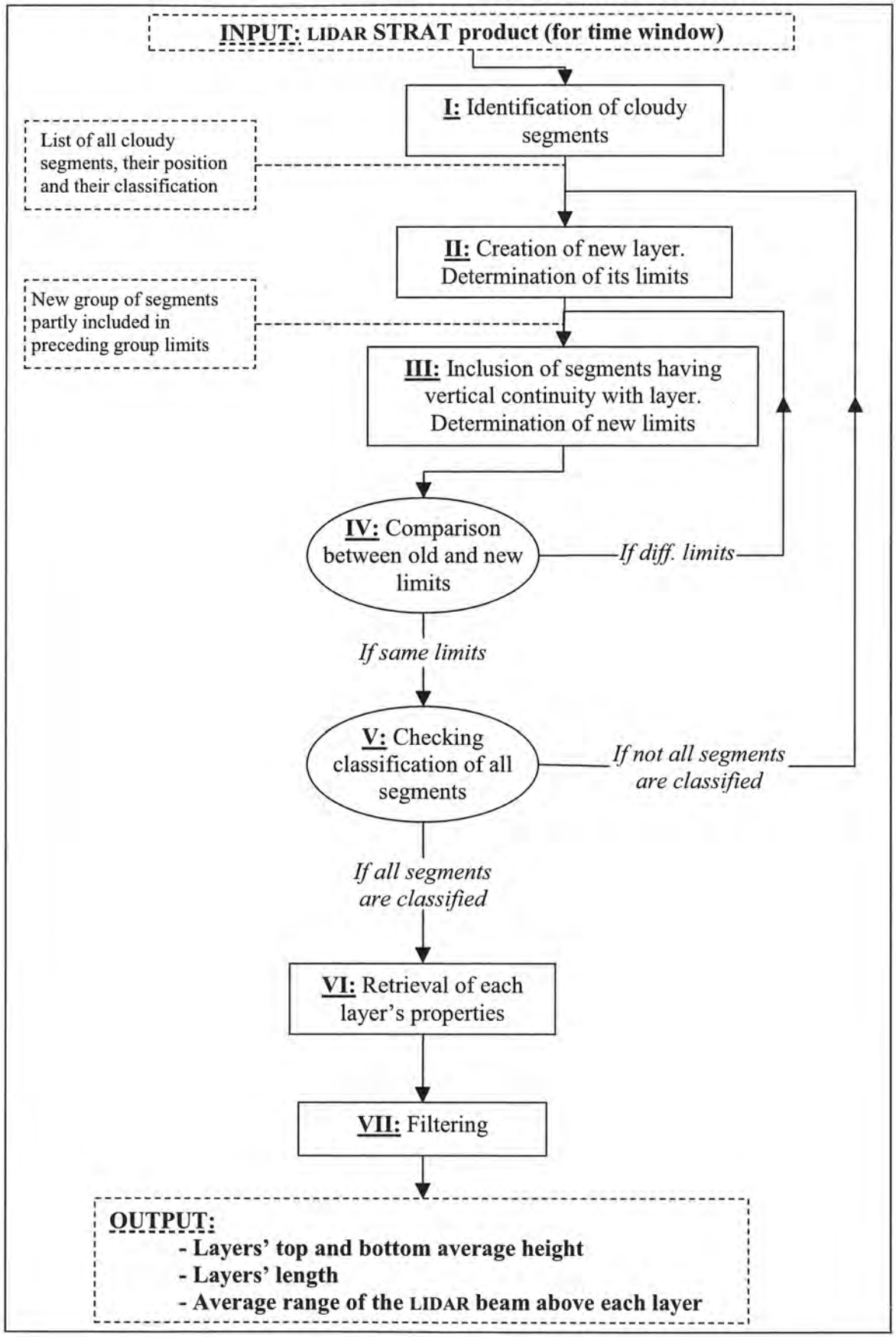

Figure 4-4 : Flowchart of the LIDAR algorithm

4.3 Cloud top height retrieval from the satellite data

4.3.a AVHRR data

In order to be coherent with the LIDAR CTH retrieval approach (identification of the different layers and retrieval of their properties separately), the CTH values retrieved by the PPS algorithm within the studied window (9x9km, centred on the SIRTA site) are grouped into different layers. An average height is then computed for each layer separately.
As mentioned in the preceding section (part III, satellite data), only the cases with at least 50% cloud coverage inside the window are included in the study.

Figure 4.3 gives the flowchart of the algorithm used to identify the different cloud layers and retrieve their properties in the AVHRR data.

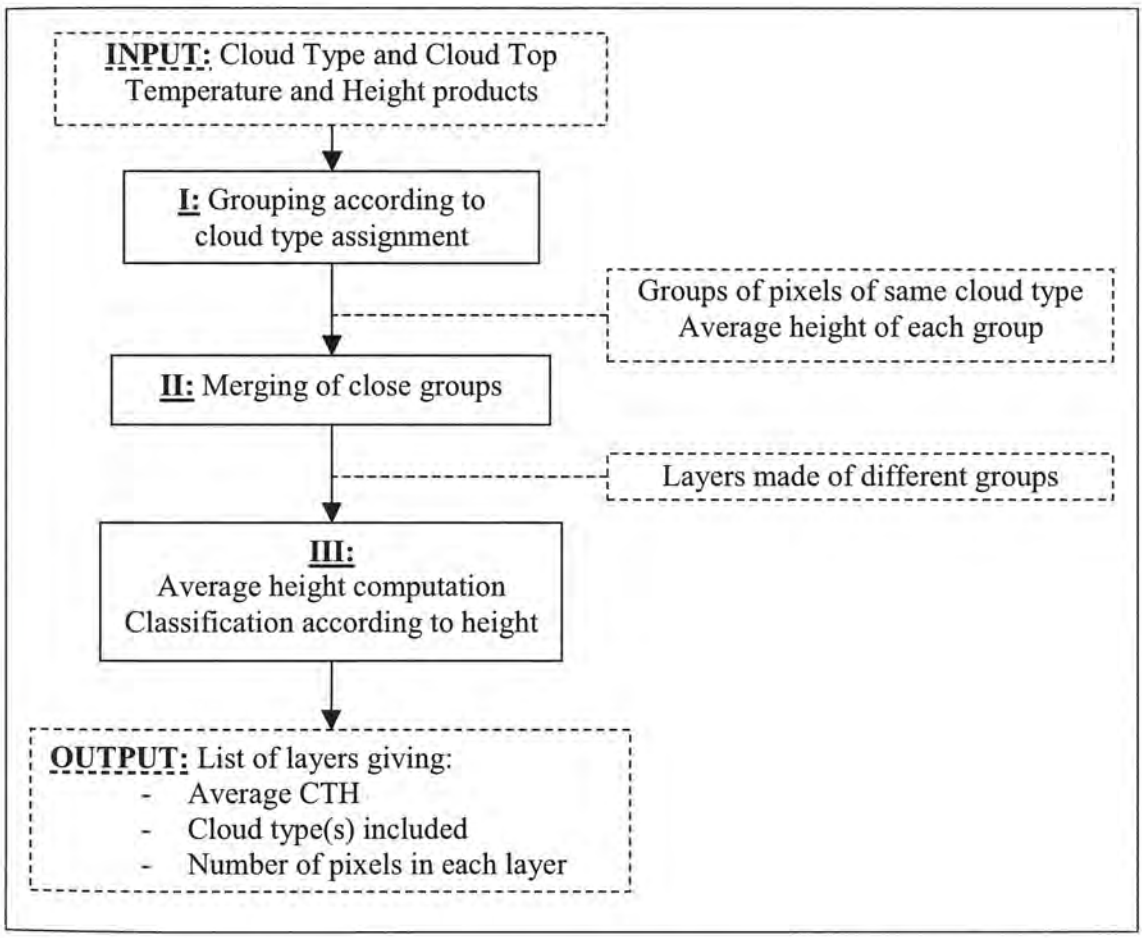

Figure 4-5 : Flowchart for the extraction of cloud layers from the AVHRR data

The identification of the different layers is made in two steps (modules I and II), then their properties are retrieved and the layers are classified according to their height (module III).

Module I
The information given by the Cloud Type product is used. We assume that, inside our window, a cloud type is found in only one cloud layer. Pixels are grouped according to their cloud type and the average height value of each group is calculated.

Module II
Groups with close heights are merged. Two groups are considered close when the difference in their height is smaller than 300 meters[1]. The groups thereby created are the different layers identified.

Module III
The average top height of each layer is computed. The layers are then classified from the highest to the lowest.

The output of this algorithm consists in a list of the different layers. For each layer, its average height, the number of pixels it includes and its type are given. At this step, only three kinds of types are considered: a layer can be semi-transparent (containing only pixels classified in a semi-transparent category by the Cloud Type product), opaque (containing only pixels classified in an opaque category by the Cloud Type product) or mixed (containing semi-transparent pixels as well as opaque pixels).

4.3.b In summary

The method described above identifies the different layers in both datasets (LIDAR and satellite). The average cloud top heights (and other parameters) are then retrieved for each layer separately. As different values are available for each scene (one for each layer), we need to link each layer identified by the satellite to the corresponding layer in the LIDAR data. When creating such pairs of layers, the goal is to ensure (as far as possible) that the height comparison is done on the same actual cloud layer. Different approaches are tested to achieve this goal. Their results are presented and discussed in the following section.

4.3.c MSG data

Above SIRTA, a MSG pixel corresponds roughly to 3 kilometres in longitude and 5 kilometres in latitude. To compare the MSG retrievals to the AVHRR ones, the test areas (spatial windows) must have approximately the same size and shape. However two conditions have to be respected when choosing a window:

-the number of pixels inside this window has to be odd so that the window is centred on the SIRTA site

-the window has to be square to be similar to the one used with the AVHRR data.

Consequently, the window used to sub-sample the MSG data measures 5x3 pixels (15x15 kilometres).

As only 15 pixels are then available for the retrieval of the MSG CTH, the approach is more straightforward. Only two possible clouds layers are considered: one corresponding to the semitransparent retrieval and one to the opaque retrieval. The CTH values are then separately averaged depending on the type of pixels.

[1] This value is to be compared to the 200 meters vertical resolution of the CTTH product. Only the layers differing by less than two CTTH units are merged in this process.

5 Results

5.1 Using dataset A

The main aim when using the LIDAR dataset A is the study of the high level semi-transparent cases. Consequently, the pairs of layers are created by linking the highest layer retrieved by the satellite to the one retrieved by the LIDAR.
Two different approaches are used to select the LIDAR layer:

- The highest layer approach.
- The closest layer approach.

5.1.a The highest layer approach

In the highest layer approach, the highest layer retrieved by the LIDAR is compared to the highest layer retrieved by the satellite. This method is consistent with the idea that the satellite, viewing the atmosphere from above, retrieves only the properties of the highest layer and is unable to see what is beneath. It is also based on the assumption that the satellite's capacity to detect thin layers is as high as the LIDAR's.

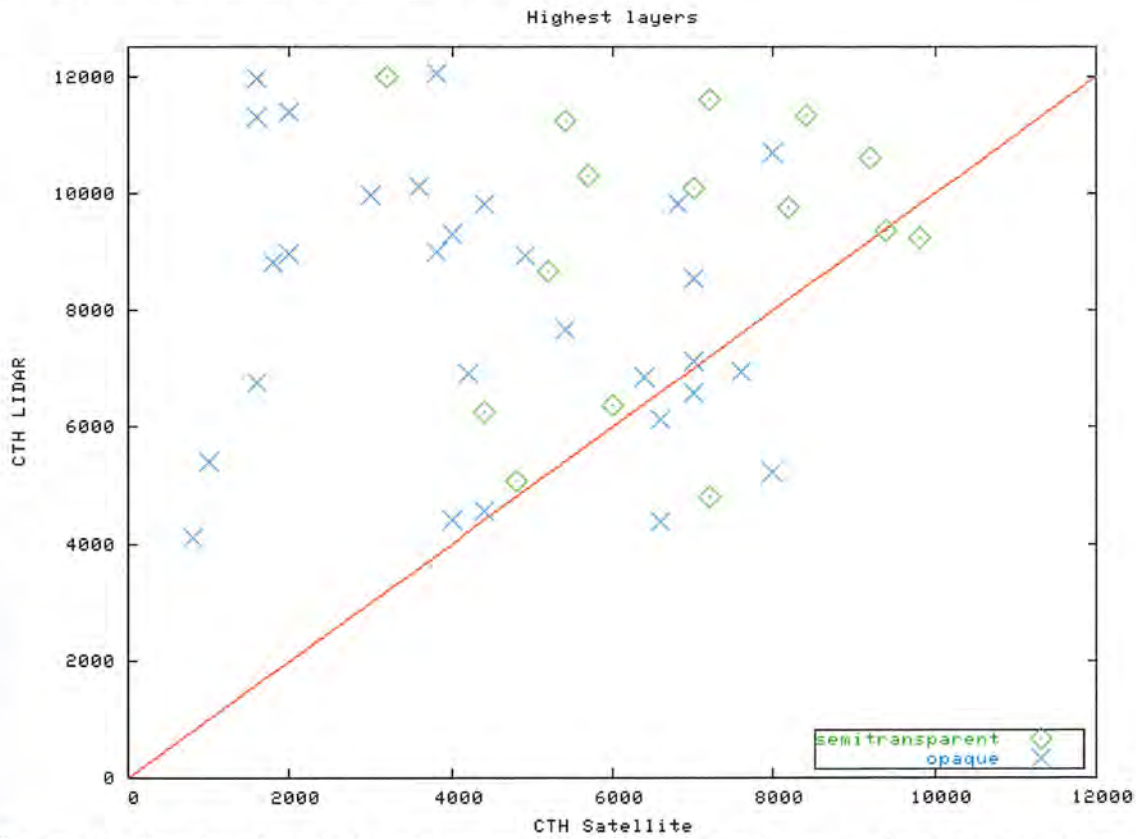

Figure 5-1 : Results of the highest layers comparison showing a systematic underestimation of the CTH by the satellite

Figure 5.1 shows the results of this comparison. We can see a nearly systematic underestimation of the cloud top height by the PPS-CTTH product both for semi-transparent and opaque cases. The linear correlation coefficient (*corr*), the average error (*bias*) and the root mean square error (σ) are presented in Table 5.1

	Nb of cases	*σ*	*bias*	*corr*
Semitransparent	15	3614m	-2368m	0.03
Opaque	29	5083m	-3613m	0.04

Table 5.1: Values of the statistical parameters for the highest layers comparison. See text for details.

This underestimation is most likely due to the inability of the PPS products to identify very thin cloud layers that are detected by the LIDAR. This inability is clear when considering, in dataset A, the cases with a satellite measurement below 4000 meters. The LIDAR highest layer is then consequently higher than the corresponding one retrieved by the satellite.

5.1.b The closest layer approach

In the closest layer approach, the highest layer retrieved by the satellite is linked to the closest layer identified by the LIDAR. This method allows selection of lower matching layers if the highest LIDAR layer is apparently invisible for the satellite retrieval. This would increase the probability of comparing the same physical layers. However, this approach would not automatically give much better results if the satellite measurement corresponds to an average CTH resulting from radiance contributions from multiple cloud layers
In this analysis, the height of the highest layer identified in the satellite data is compared to the height of each layer identified in the LIDAR data. The closest layer identified in the LIDAR data is kept for comparison.

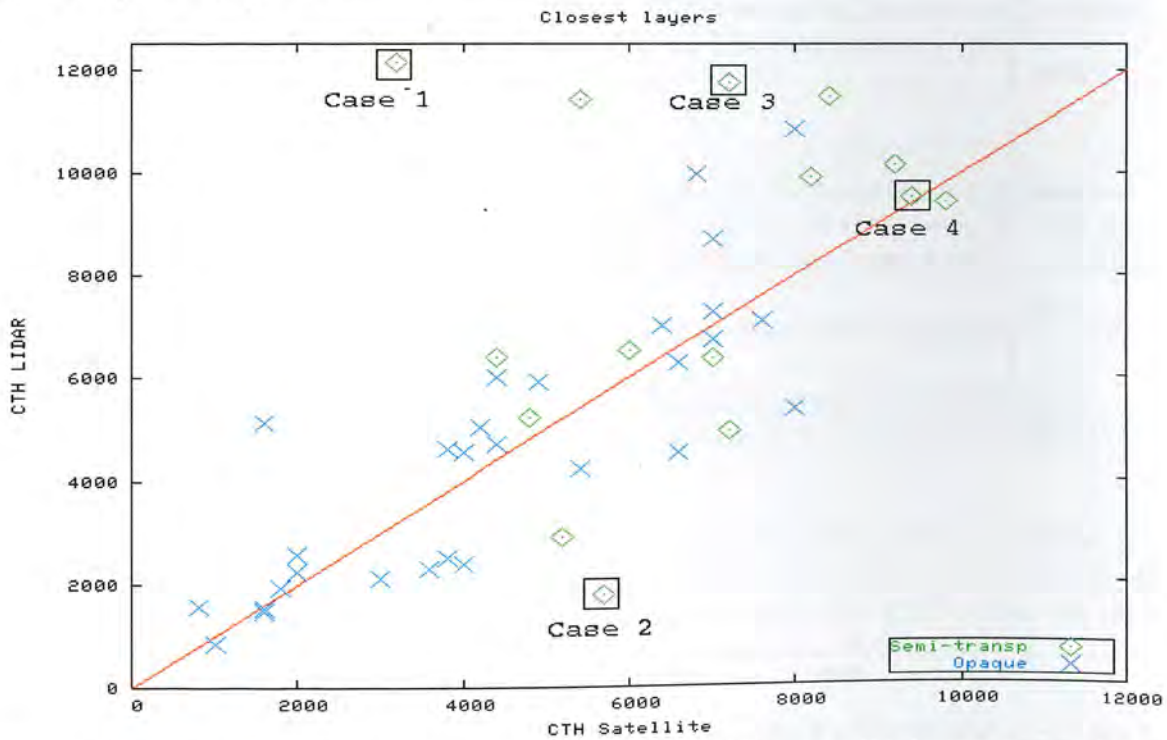

Figure 5-2 : Results of the closest layer comparison made on the highest satellite layer showing a better agreement between the two datasets. The cases selected will be analyzed further.

Figure 5.2 shows the results of this comparison. It shows a better agreement between the two datasets resulting in better linear correlation coefficients (*corr*), bias error (*bias*) and root

mean square errors (σ) than the ones obtained in the highest layer approach. Refer to Table 5.2 for values

	Nb of cases	σ	*bias*	*corr*
Semitransparent	15	3416m	-1097m	0.09
Opaque	29	1426m	-73m	0.70

Table 5.2: Values of the statistical parameters for the highest layers comparison. See text for details.

The better agreement found for the opaque cases and the improvement in the bias error for the semitransparent cases in the closest layer approach support the view of the inability of the PPS products to identify the thinnest cloud layers yet identified by the LIDAR. The CTTH product still tends to underestimate the cloud top height, especially in the case of semi-transparent clouds.

5.1.c Visual inspection of worst cases

In order to understand the reasons of the underestimation of the CTH in cases of semitransparent clouds, a visual inspection of the some selected cases is performed (cases marked in boxes in Figure 5-2). This study is carried out on 6 worst cases and one good case. The results of this analysis are presented below for 3 worst cases (cases 1, 2 and 3) and one good case (considered to be the most representative of the situations leading to a good retrieval).

For each satellite scene, a picture of the LIDAR data is given as well as four different satellite pictures following the model below.

Composite RGB picture of AVHRR channels 1, 2 and 4.	Composite RGB picture of AVHRR channels 3, 4 and 5.
Cloud Type product	Cloud Top Temperature and Height product

In order to have an idea of the general cloud system, each picture shows the situation in a 200km by 200km area around the SIRTA site. The test area of 9x9km is drawn in white. The 32x32 pixels wide image segment, used by the histogram method, is drawn in dashed white. Figure V-3 gives the colour codes for the CT and the CTTH products and for the LIDAR data.

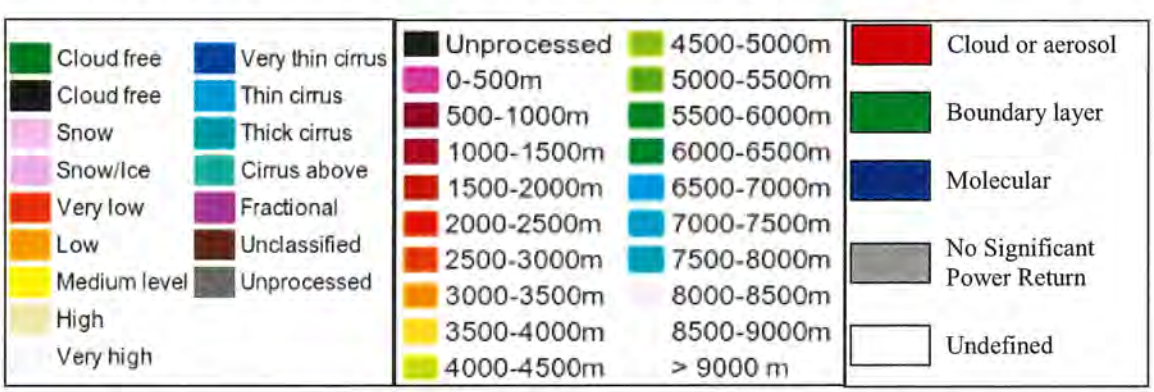

Figure 5-3: Colour codes for the CT product (left), the CTTH product (middle) and for the LIDAR data (right)

Case 1: 18th May 2004 at 12h15 (Figure 5-4 and Figure 5-5 on page 25)

In this case, the CTTH product retrieves a CTH of 3200 meters while the LIDAR retrieves an average CTH of 12140 meters and no lower level clouds (Figure 5-5).
On the satellite composite images, one can hardly see any cloud in the window of study. These clouds are extremely thin and are at the limit of detection for the PPS product.
Some lower level clouds are visible inside the image segment used by the histogram method (large orange square in CTTH picture). In the Cloud Type product, these are identified as fractional clouds.

Case 2: 21st May 2003 at 9h27 (Figure 5-6 and Figure 5-7 on page 26)

In this case, the CTTH product retrieves a CTH of 5700 meters while the LIDAR retrieves an average CTH of 1778 meters.
In the LIDAR dataset, two cloud layers are identified: one at 1778 meters (used for comparison) and one around 10500 meters.
As the method used is the closest layer approach, the algorithm compares the satellite-retrieved CTH to the CTH of the lower layer because it is closer than the highest one. A visual inspection shows that the semitransparent layer is actually the highest one and that the lower layer is opaque. Consequently, this case should in reality also be considered as an underestimation of the CTH by the semitransparent algorithm.
It should also be noted that a few pixels belonging to the low level cloud layer are classified as fractional clouds.

Case 3: 25th May 2004 at 16h41 (Figure 5-8 and Figure 5-9 on page 27)

In this case, the CTTH product retrieves a CTH of 7200 meters and the LIDAR retrieves an average CTH of 11740 meters.
On the picture of the LIDAR data, some lower level clouds, located at the top of the boundary layer, are partly identified (small red segments).
On the satellite composite images, the thin layer is hardly visible while a lower level cloud system is clearly identified in the vicinity of the test area. Inside the image segment used by the semitransparent algorithm, these lower level clouds are classified as fractional clouds by the CT product.

Case 4: 16th April 2004 at 17h01(Figure 5-10and Figure 5-11 on page 28)

This case is an example of a good retrieval: the CTTH product retrieved a CTH of 9400 meters and the LIDAR retrieves a CTH at 9500 meters.
The images show the main difference with the preceding cases: the absence of any sight of lower level clouds inside the image segment used by the semitransparent algorithm. As well, the cloud identified as semitransparent is as well thicker than in the preceding cases. The latter could explain the improved success of the method despite the fact that the LIDAR actually indicates the presence of very thin low level clouds.

Case 1: 18th May 2004, 12h15

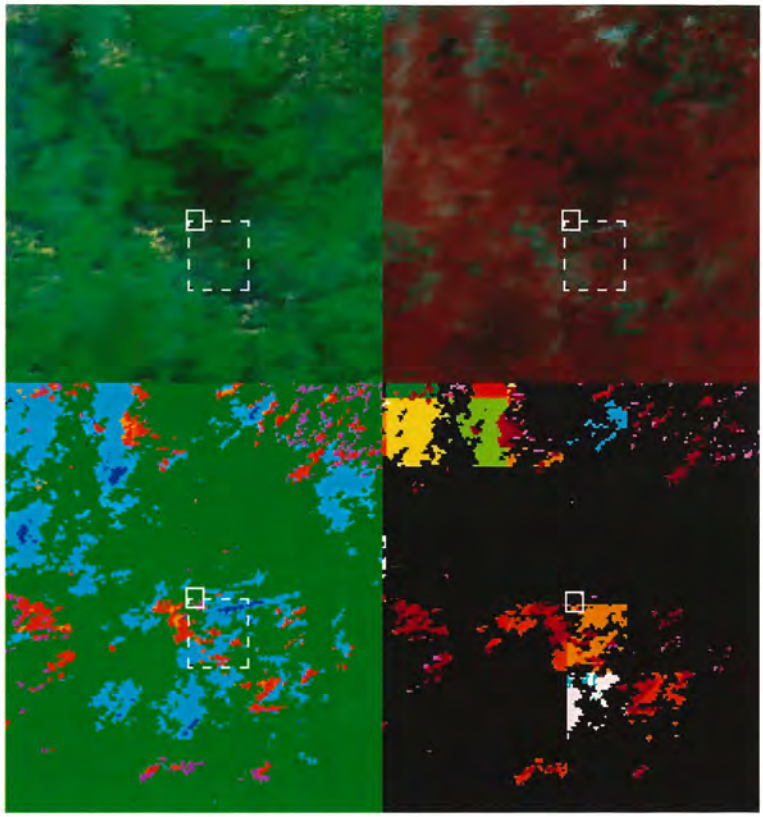

Figure 5-4 : Satellite scenes of the 18th May 2004 at 12h15 above SIRTA (see page 23 for details). The thin cirrus detected in the test area are hardly visible and the scene is contaminated with lower level clouds classified as fractional clouds.

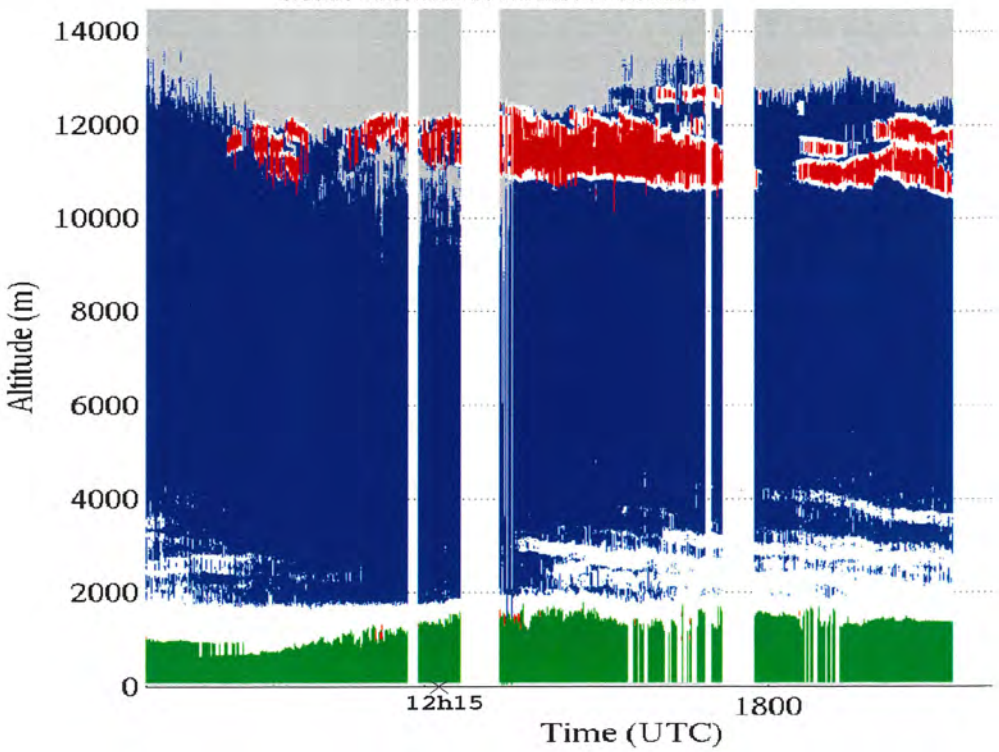

Figure 5-5: LIDAR data for the 18th May 2004 (see Figure 5-3 for colour code). Around 12h15, only one cloud layer (with its top around 12000 m) is detected.

Case 2: 21st May 2003, 9h27

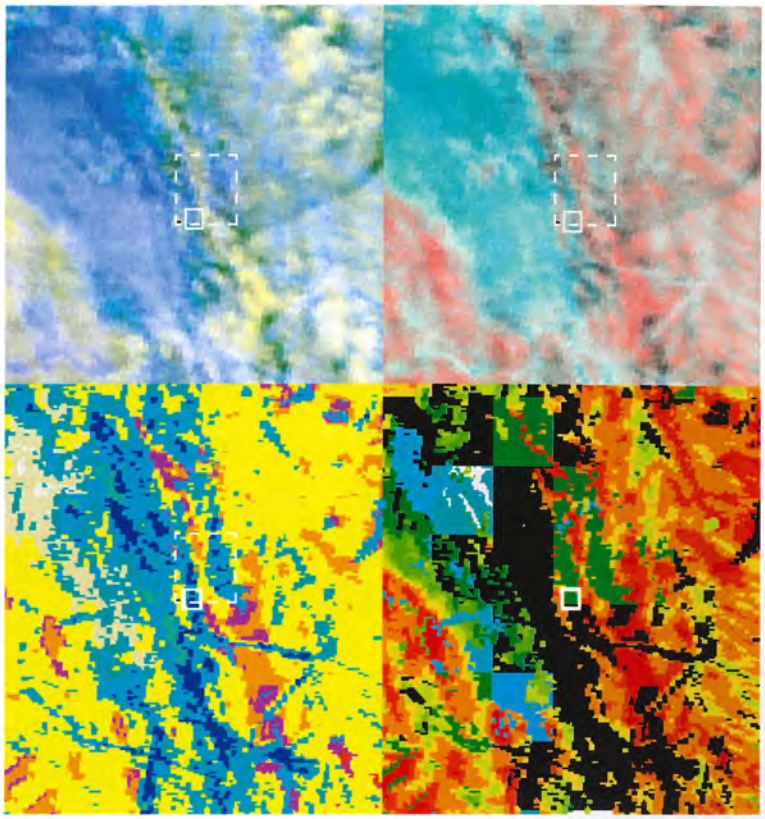

Figure 5-6: Satellite scenes of the 21st May 2003 at 9h27 above SIRTA (see page 23 for details). Inside the image segment used to perform the histogram method, low level clouds persist underneath the cirrus layer. Inside this segment, a few pixels are classified as fractional clouds.

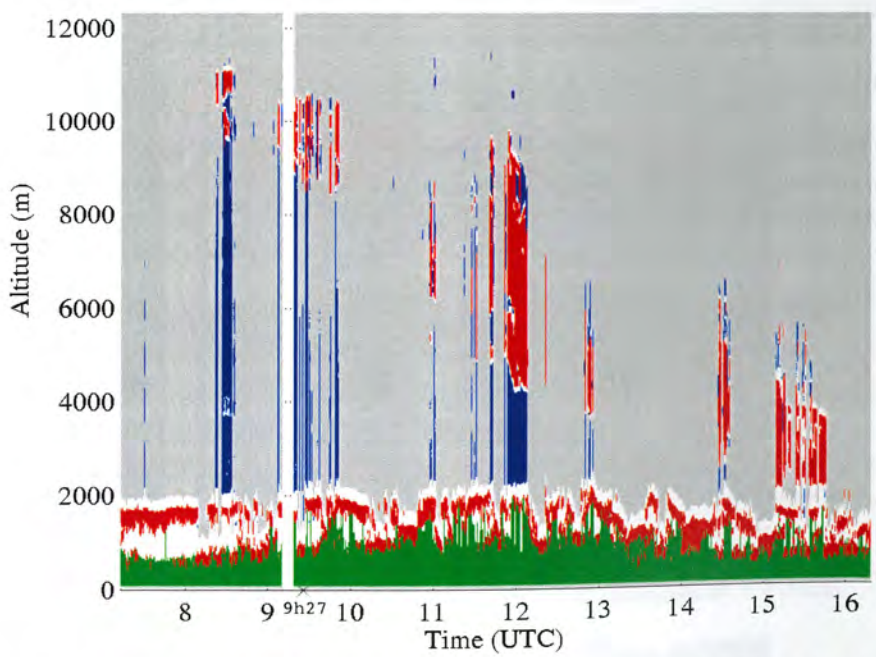

Figure 5-7: LIDAR data for the 21st May 2003 (see Figure 5-3 for colour code). Some low level clouds persist during all the day and higher clouds are only partly retrieved. At 9h27, some high level clouds are identified.

Case 3: 25th May 2004, 16h41

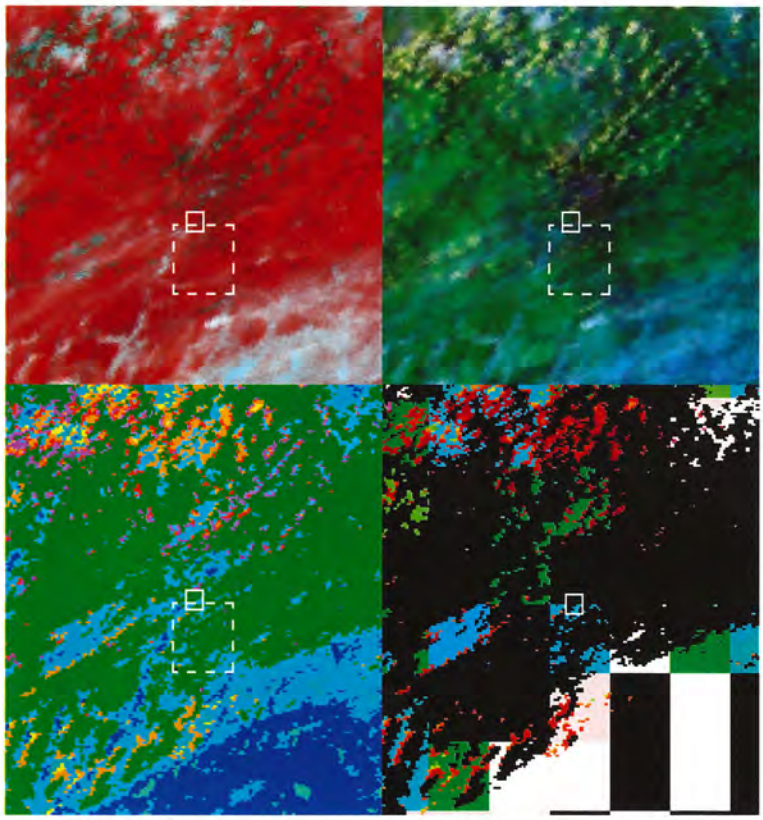

Figure 5-8: Satellite pictures of the 25th May 2004 at 16h41(see page 23 for details) above SIRTA. The identified thin cirrus are very thin and cover only partially the test area.

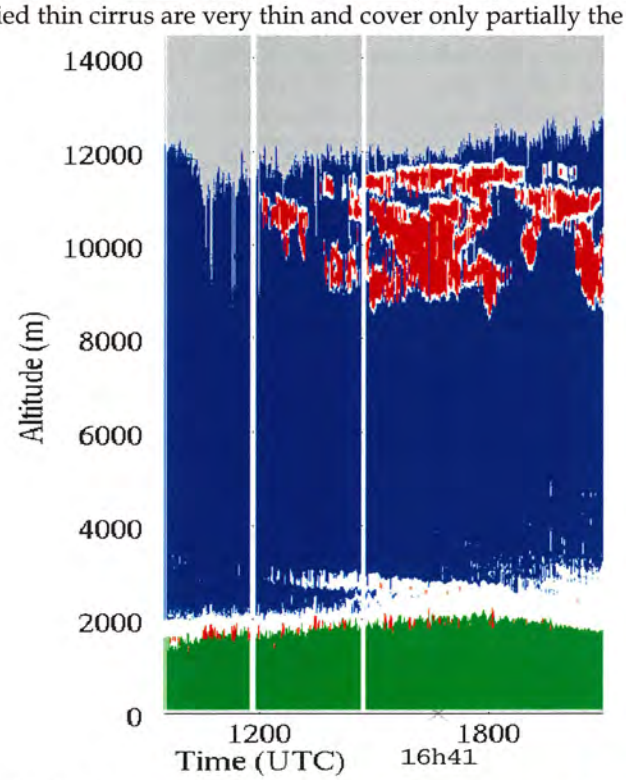

Figure 5-9: LIDAR data for the 25th May 2004 (see Figure 5-3 for colour code). Around 16h41, high level clouds are identified. Lower level clouds at the top of the boundary layer are also partly identified.

Cases 4: 16th April 2004, 17h01

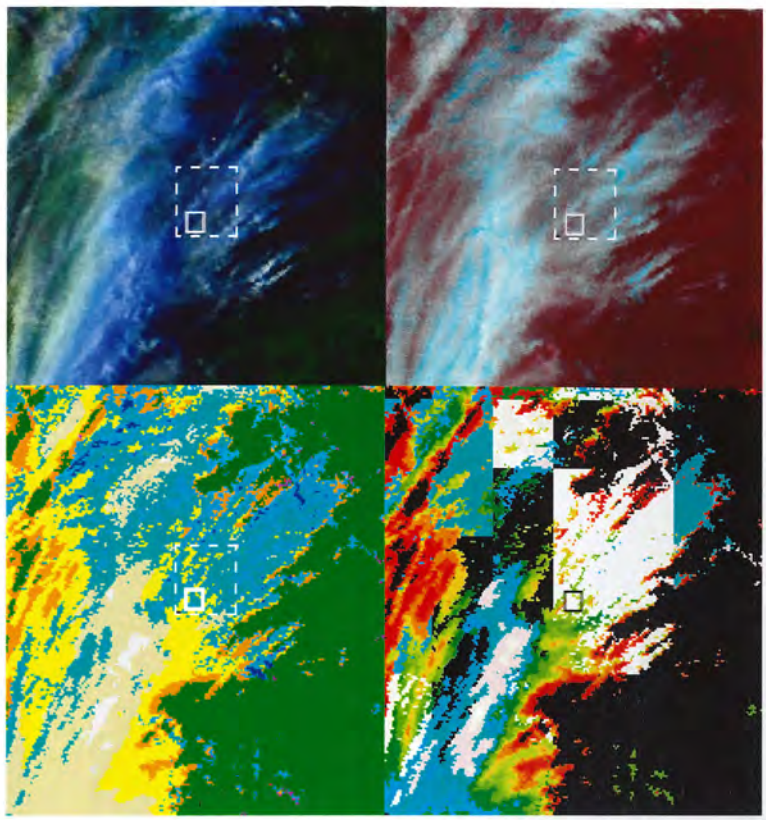

Figure 5-10: Satellite pictures of the 16th April 2004 at 17h01 (see page 23 for details) above SIRTA. The cirrus cloud is quite dense and no lower level fractional clouds are identified inside the image segment used by the semitransparent algorithm.

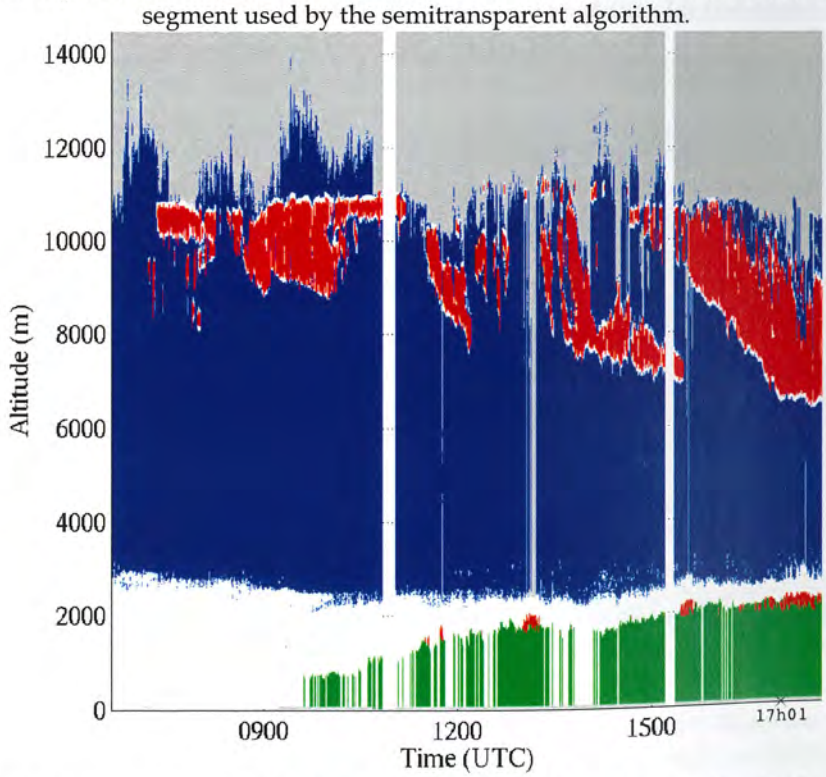

Figure 5-11: LIDAR data for the 16th April 2004. At 17h01 a high level cloud layer is identified as well as a lower level one. The higher level one seems continuous.

5.1.d A possible explanation for the underestimation of the CTH by the semitransparent algorithm

From the preceding visual inspection, when the PPS algorithm for semitransparent clouds underestimated the CTH, it seemed that the following scenario occurred: a very very thin cirrus (hardly visible on the composite images) was identified and lower level clouds, classified as fractional clouds by the Cloud Type product, existed in the vicinity of the test area. The reasons for the underestimation become clear when studying such a scenario in the $(T_4-T_5)/T_4$ histogram. It appears to be the result of a combined effect of the presence of very thin semi-transparent clouds and the presence of lower level fractional clouds.

The general shape of the histogram for a semitransparent cloud layer is an arc shaped curve opening downwards. The left part of the curve represents the opaque pixels and intercepts the x-axis at the CTT while the right part of the curve represents the nearly transparent pixels and intercepts the x-axis at the surface temperature. The semitransparent method is based on the fitting of the data to this theoretical curve [Korpela et al. 2001]. To ensure a proper fitting, a case is processed only if the data is sufficiently distributed (according to width) horizontally.

When two cloud layers are identified at different levels as described above, the data is distributed in two distinct groups of pixels, one for each layer (Figure 5-12).

The first group (green dots on the figure) corresponds to the semitransparent high level layer and is located on the right part of the histogram. As this layer is very thin, the horizontal distribution of the data is restricted to the right part (transparent part) of the curve corresponding to this layer (green dashed line), allowing various possible fits.

The second group (blue dots on the figure) corresponds to the lower level fractional cloud layer. As this layer is more opaque (water clouds), the data corresponds to the left part of the theoretical curve (opaque part). It must be noted that the number of pixels part of the second group is far smaller than the number of pixels in the first group (higher layer, green dots). The first group is consequently much more important for the fitting.

When processing such a case, the algorithm fails in the CTT retrieval because it was not developed for multilayer situations. Consequently, these two groups are incorrectly interpreted as part of one unique layer. The algorithm fits a theoretical curve to this data, consequently leading to an estimated CTT located between the actual CTT values of the two layers.

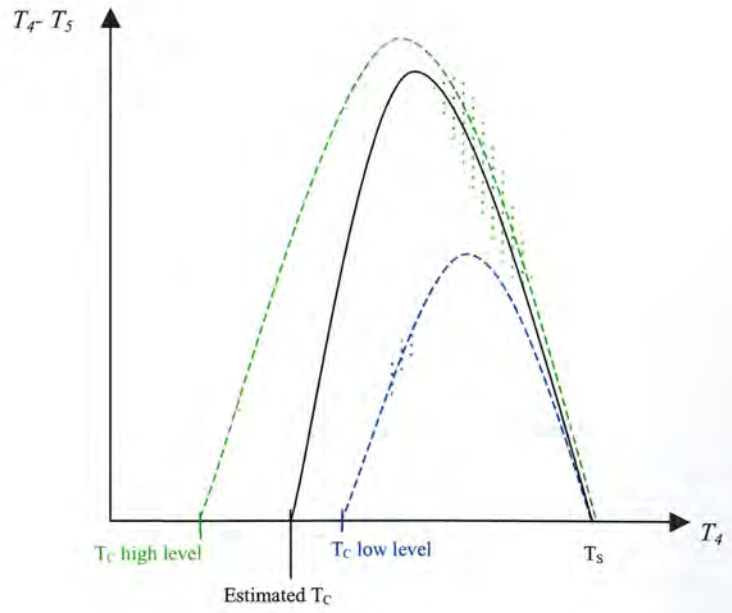

Figure 5-12: (T_4-T_5) vs.T_4 histogram giving a schematic representation of the situation leading to an underestimation in the Cloud Top Temperature. T_C is the brightness temperature of the cloud top (in channel 4) and T_S is the surface brightness temperature. The green dashed lined represents the theoretical curve for the higher level semitransparent clouds; the blue dashed one for the lower level fractional layer. The green (resp. blue) dots correspond to the high level (resp. low level) layer. The black line is the result of the fitting. The algorithm finds a solution (black line) that is a mix of both layers.

5.2 Using dataset B

To validate the CTTH retrieval for low level water clouds, dataset B is used. This dataset includes only the cases where no layer was identified by the LIDAR above 4000 meters. As the LIDAR beam is stopped by water clouds, dataset B includes most of the cases where those clouds were identified. The comparison is made by using the best agreement approach.

The best agreement approach

The best agreement approach aims to ensure that the height comparison is done on the same physical layer when no information is available above the cloud. Indeed, when low level water clouds are present, the LIDAR is often unable to retrieve the atmospheric properties above them.

In this approach, each layer identified by the satellite is compared to all the layers identified by the LIDAR. As in the closest layer approach, each satellite layer is linked to the closest LIDAR layer. Then, the set of pairs thereby created is analyzed to find the one giving the best agreement between the two retrievals. This pair is kept for comparison.

This method, if applied to the whole LIDAR dataset, tends to overestimate the performance of the CTTH product as it only keeps for comparison the best values available for each scene. Nevertheless, when considering the dataset B, which only includes values with low level water clouds and with very little information about the state of the atmosphere above them, this method is the best way to search the datasets for corresponding layers.

The results of this comparison are shown in Figure 5-13.

As expected, in some cases the height retrieved by the LIDAR is much smaller than the one retrieved by the satellite. The explanation for this lies in the inability of the LIDAR to reach the cloud tops and to retrieve information about the highest layers. This comparison illustrates the need to filter the LIDAR dataset (into dataset A and dataset B) in order to ensure reliable measurements.

	Nb of cases	*σ*	*bias*	*corr*
Semitransparent	4	1049m	747m	0.67
Opaque	44	1338m	420m	0.20

Table 5.3: Standard deviation (□), bias and correlation found for lower level cloud layers (dataset B).

The correlation found for the semi-transparent cases is very good (0.67). Even if limited (given the very limited number of cases), this result tends to show that the semitransparent method works well for fractional cloud situations. In these cases, the number of pixels inside the image segment used by the histogram method is large enough to ensure a good fitting of the theoretical curve to the data.

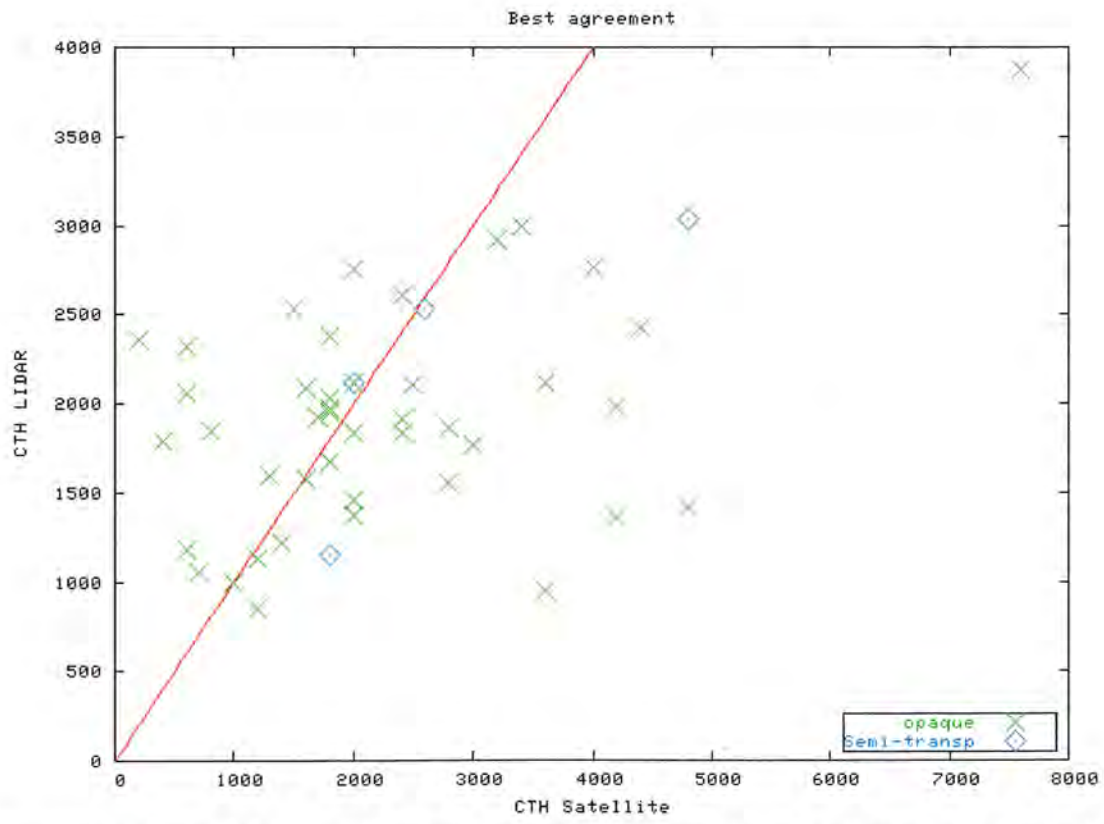

Figure 5-13: Results of the comparison for the lower level cloud layers. In many cases, as the LIDAR doesn't reach the cloud top, it returns a smaller CTH value than the satellite. For the fractional clouds (semitransparent algorithm), the results show a good agreement between the two datasets but only four cases are available.

5.3 Comparison with the values retrieved by MSG-SEVIRI

When comparing the values retrieved by AVHRR to the ones retrieved by SEVIRI, the highest layer approach is used (the highest layer identified in the LIDAR data is compared to the highest layer retrieved by the satellite, see section 5.1). As this approach is straightforward, it allows comparison between one LIDAR retrieval and two different satellite measurements. Consequently, when plotting the results, a defined scene is represented by two dots (one for the AVHRR measurement and one for the SEVIRI measurement) with the same CTH LIDAR value. Figure 5-14 shows the results of this comparison. Only the scenes with both an AVHRR and a SEVIRI measurement are plotted.

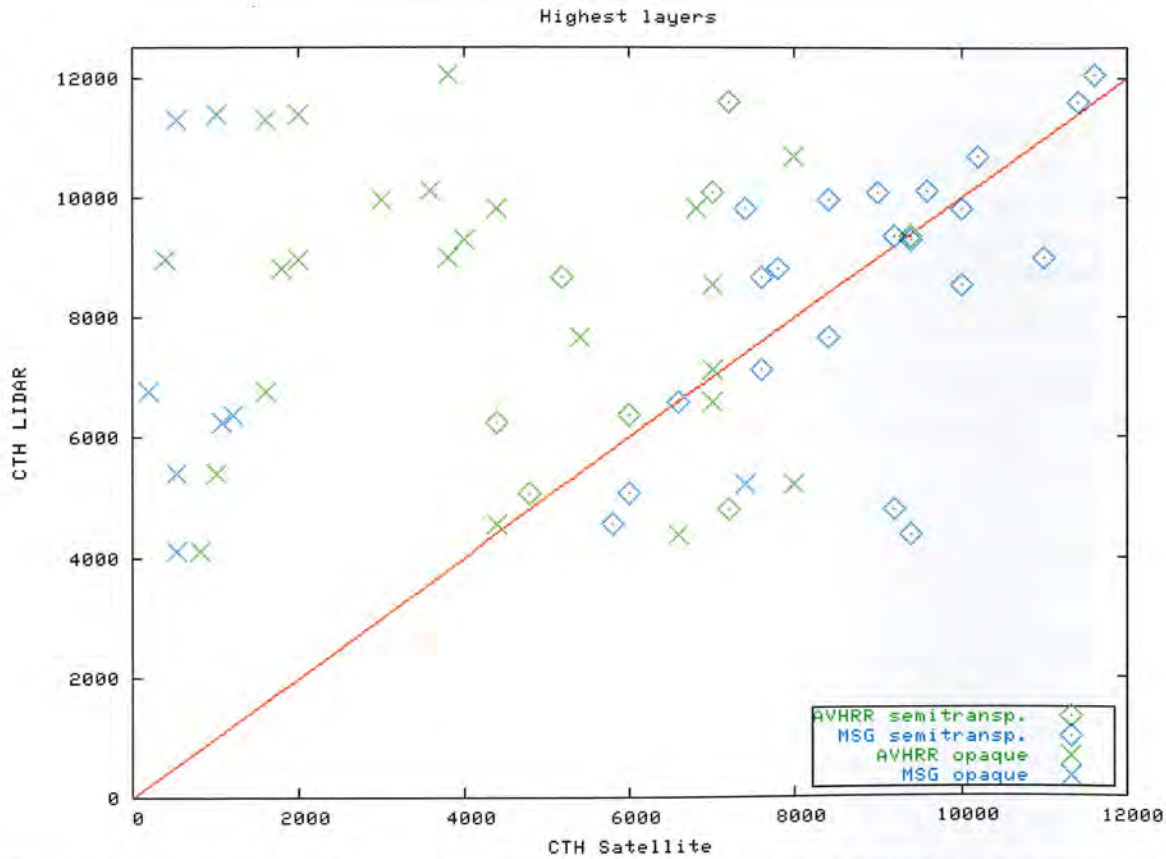

Figure 5-14: Results of the inter-comparison between AVHRR and SEVIRI retrievals using the highest layer approach. A larger number of semitransparent cases are seen in the SEVIRI data and opaque retrievals seem to show no agreement with the LIDAR retrievals. This raises the question of parallax problems in the SEVIRI data.

Figure 5-14 shows two distinct groups of SEVIRI retrievals: semitransparent cases, which present a good agreement with the LIDAR retrievals, and opaque cases, which seem to present no correlation with the LIDAR retrievals. The values of the linear correlation coefficient (*corr*), bias error (*bias*) and standard deviation (σ) for both instruments are presented in Table 5.4.

	Nb of cases		*σ*		*bias*		*corr*	
	AVHRR	MSG	AVHRR	MSG	AVHRR	MSG	AVHRR	MSG
Semitransparent	15	21	3614m	1778m	-2368m	363m	0.03	0.39
Opaque	29	9	5083m	6955m	-3613m	-5880m	0.04	0.08

Table 5.4: Statistical values for the inter-comparison. See text for details.

Figure 5-14 and Table 5.4 show a major difference between AVHRR and SEVIRI retrievals: it lies in the number of clouds classified as semitransparent. In the data subset used for this inter-comparison (30 cases), AVHRR identifies only 8 scenes as filled with semitransparent clouds while SEVIRI identifies 21 scenes. These cases show as well a better agreement with the LIDAR retrievals than the AVHRR semitransparent retrievals. This better agreement indicates a higher ability of the MSG SEVIRI instrument to detect high level semitransparent clouds.

The reason for the difference can be a higher sensitivity of the SEVIRI sensor with respect to thin clouds but it can as well be largely explained by the differences in the viewing conditions of the two satellites. Indeed, as MSG is a geostationary satellite, it observes the SIRTA location (mid-latitudes) with a much larger viewing angle than NOAA polar satellites (that perform measurements more closely to nadir). When seen from a slanted view, semitransparent clouds seem much thicker and consequently have a much larger impact on the measured radiances.

However, this effect should also lead to a higher number of semitransparent clouds being interpreted as opaque by SEVIRI than by AVHR. A possible explanation for the observed results (larger number of semitransparent cases in SEVIRI data) lies in a combined effect of the different viewing angles and the high altitude of the semi-transparent clouds. Because of parallax errors, high level clouds located south of SIRTA could be erroneously placed over SIRTA location. As this displacement does not occur in the same systematic way with AVHRR, the measurements are not actually performed on the same targets. AVHRR can perform a measurement on a multiple cloud layer situation (which lead to a misclassification of semitransparent clouds as opaque, see section 5.1) while SEVIRI only targets at a thin cloud, therefore classifying it correctly (see Figure 5-15).

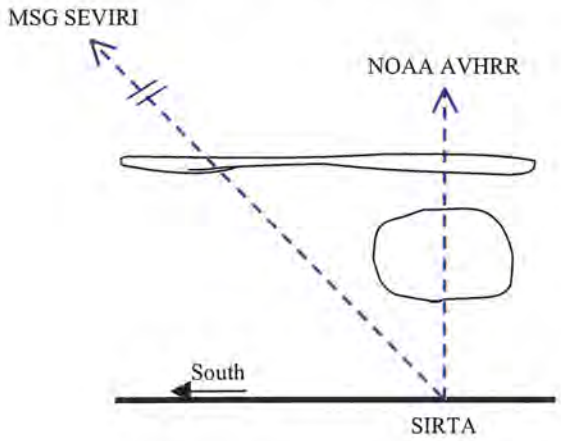

Figure 5-15: Schematic representation of a possible explanation for the greater number of semitransparent cases observed in the SEVIRI data. While AVHRR targets a multilayer cloud situation, SEVIRI targets a high level thin cloud.

The values found for the opaque cases are quite surprising. Indeed, the retrieval method used for opaque clouds is supposed to be very reliable. Again, the phenomenon described above can explain the results. It is very likely that the low level opaque clouds identified by SEVIRI are present above SIRTA in a multiple layer cloud situation but that the higher clouds identified by the LIDAR are projected further north in the SEVIRI data.
If this explanation is correct, then the low level clouds identified in the SEVIRI data should as well be identified in the LIDAR data. To check this assumption, the closest layer approach is applied on these 8 cases: each time the SEVIRI retrieval is linked to the closest cloud layer identified in the LIDAR data (and not with the highest layer anymore, see part 5.1). The results are presented in Figure 5-16.
In 7 of 8 cases, a low level cloud is identified in the LIDAR data. This result supports the explanation given above.

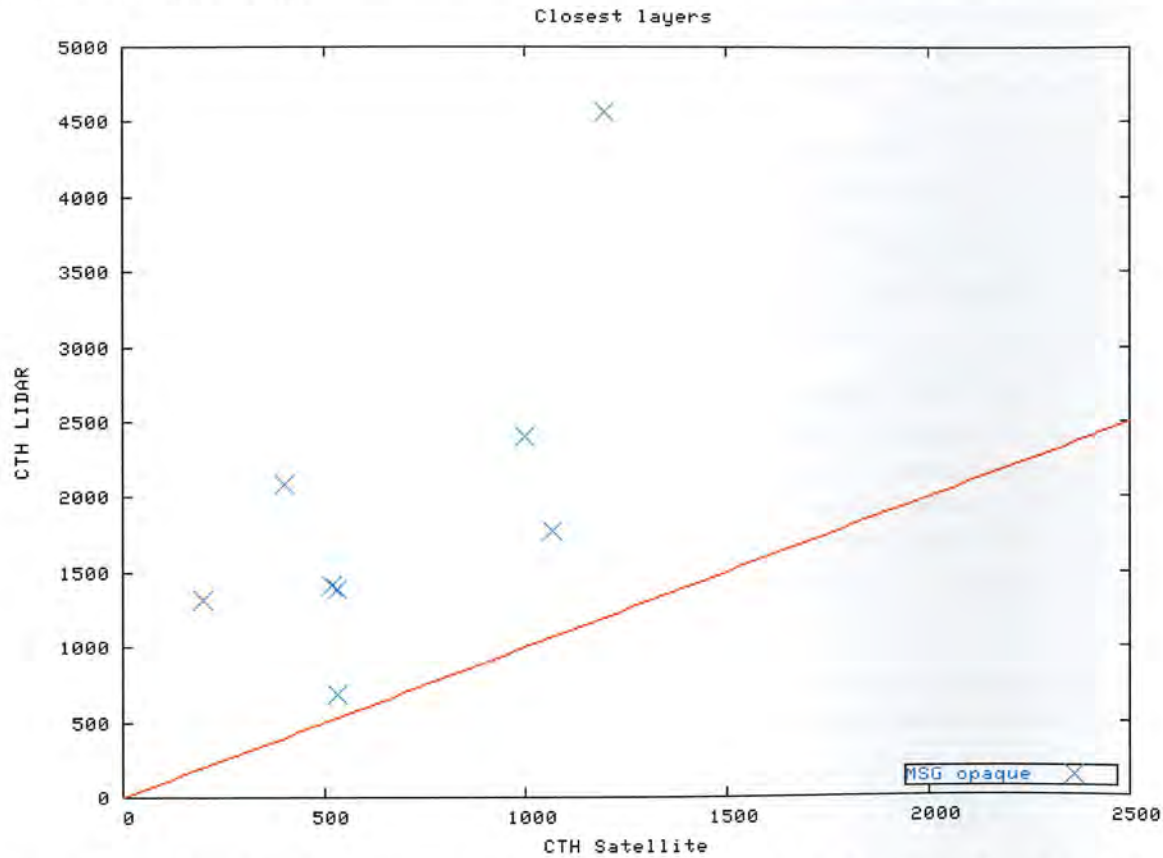

Figure 5-16: Closest layer approach applied on MSG opaque cases. A low level cloud layer is as well identified in the LIDAR data. This result tends to confirm that high level clouds are mislocated in the MSG data.

In summary, this first comparison between AVHRR and SEVIRI retrievals shows a better ability of SEVIRI to identify thin clouds; it is largely explained by the differences in the viewing conditions of the two satellites. However, the large viewing angle of MSG leads to a displacement of high level clouds further north (in this hemisphere). This problem leads to major difficulties when trying to compare NOAA and MSG measurements as the sensors onboard the two satellites don't actually target the same situations. It also underlines the fact that great care should be taken with the location when interpreting MSG results for high level clouds.

6 Conclusion

This study is a validation of the SAFNWC PPS CTTH product for semitransparent clouds using LIDAR data. It as well gives a preliminary comparison with the results of the SEVIRI algorithm.
An automated method for comparing satellite and LIDAR datasets is introduced. This method automatically identifies the different cloud layers in the LIDAR data pre-processed by the STRAT algorithm (from SIRTA), and retrieves their heights separately. A similar method is used to process the AVHRR satellite data, using the Cloud Type and the CTTH products. Different approaches are then used to compare the two datasets.

The efficiency of the method is estimated in the first place. This is done by comparing the number of cases labelled as semitransparent clouds (by the Cloud Type product) to the corresponding final number of CTTH retrievals in this particular cloud group. For the period of study, 27% of the cloud classified as semitransparent by the Cloud Type product had their CTH retrieved by the CTTH product.

Comparing LIDAR data to satellite retrievals is not straightforward and often problematic. This is due to the opposing locations of the two instruments with respect to the atmosphere (the LIDAR is ground based, the satellite is above the atmosphere) and to their different sensitivities to the opacity of the targets (the LIDAR is very sensible, the satellite sensor less).
In many cases, when low level water clouds are present, the LIDAR does not retrieve the properties of the atmosphere above the lower layer. Indeed, the LIDAR beam is stopped when the clouds are too opaque. To overcome this problem, the LIDAR data is split in two parts according to the height of the highest retrieval (above or below 4000m), assuming that high level clouds are optically thin enough to guarantee a reliable dataset.
However, semitransparent clouds are well identified and their CTH is precisely retrieved by the LIDAR which make the LIDAR data very useful.

The first dataset contains the LIDAR retrievals for high cloud layers. It is used for the study of high level semitransparent cases.
When comparing the height of the highest cloud layers retrieved by both instruments, a systematic underestimation of the cloud top height by the PPS algorithm is revealed. This seems to be due to the inability of the AVHRR instrument to detect the thinnest cloud layers which are, however, clearly identified in the LIDAR data.
When comparing the height of the highest cloud layer retrieved by the PPS algorithm to the closest one found in the LIDAR data, a better agreement between the two datasets is found. This result tends to confirm the inability of the AVHRR instrument to detect very thin high-level clouds. It also shows that when some conditions are fulfilled (a single cloud layer thick enough to ensure significant data), the algorithm retrieves a correct CTH. However, some cases still show an underestimation of the CTH.
When performing a visual inspection of these cases, similar cloud situations are often found. The underestimation occurs mainly in multilayer situations with the highest layer being very very thin and the lowest layer being fractional. When such a case is processed, values from both layers are used by the semitransparent algorithm as if only one layer was present. This is because both types of clouds are considered semitransparent in the PPS algorithm. Consequently, the CTH estimation is a mix of the actual CTH values of the two different layers.

The second dataset is expected to contain only cases with lower level water clouds and no LIDAR retrieval above 4000m. It is used in an attempt to validate the CTTH product for lower level fractional clouds. It also illustrates the need to split the LIDAR dataset in order to select reliable measurements (dataset A). The results are interpreted with great care as the LIDAR data is then considered to be not very reliable. However, for cases classified as semitransparent or fractional clouds by the Cloud Type product, the correlation between the two datasets is quite good. Even if this result has to be taken with care provided the very small number of cases available for study, it tends to show that the semitransparent correction in case of fractional clouds works well.

The comparison between AVHRR and SEVIRI results is not straightforward. The very large viewing angle of the SEVIRI sensor (onboard MSG) leads to a displacement of high clouds (parallax error) with various consequences: high level clouds south of the SIRTA site are incorrectly located at SIRTA's location in the SEVIRI data, high level clouds above the SIRTA site are located further north. Consequently the two instruments don't target at the same situations. However, the SEVIRI algorithm seems to be more able to detect thin clouds as they appear thicker than they actually are when viewed slantwise.

REFERENCES

Brunel, P. and Marsouin, A., 2000: Operational AVHRR navigation results. Int. J. of Remote Sensing, vol. 21, no. 5, 951-972

Derrien, M., L. Lavanant, and H. L. Gléau, 1988, Retrieval of the cloud top temperature of semi-transparent clouds with AVHRR, in Proceedings of the IRS'88, Lille, France, pp. 199–202.

Dybbroe, A., Karlsson, K.-G., and Thoss, A., 2005a, AVHRR cloud detection and analysis using dynamic thresholds and radiative transfer modeling – part one: Algorithm description, Journal of Applied Meteorology, in press, to appear 2005.

Dybbroe, A., Karlsson, K.-G., and Thoss, A., 2005b, AVHRR cloud detection and analysis using dynamic thresholds and radiative transfer modeling – part two: Tuning and Validation, Journal of Applied Meteorology, in press, to appear 2005.

Eyre, J. R., 1991, A fast radiative transfer model for satellite sounding systems. Technical Memorandum 176, ECMWF. Available from the librarian at ECMWF.

Haeffelin M., L. Barthès, O. Bock, and al., 2005, SIRTA, a ground based atmospheric observatory for cloud and aerosol research, Annales Geophysicae, in press, to appear 2005.

Inoue, T., 1985, On the temperature and effective emissivity determination of semi-transparent cirrus clouds by bi-spectral measurements in the 10μm window region. J. Met. Soc. Japan, 63, 88–98.

Joro S. and Dybbroe A., 2004, Validating the AVHRR Cloud Top Temperature and Height product using weather radar data, Visiting Scientist report, SMHI.

Karlsson et al., 2004, CM-SAF ORRV1 validation report for basic cloud products (CFC/CTY/CTT/CTH), SMHI, Document SAF/CMSMHI/CFC-CTH-1.

Korpela A, A. Dybbroe and A. Thoss, 2001, Retrieving Cloud Top Temperature and Height in Semi-transparent and Fractional Cloudiness using AVHRR. Visiting Scientist Report, National Institute of Water and Atmospheric Research, New Zealand & SMHI.

Le Gléau Hervé, 2004, Software User manual of the SAFNWC / MSG : Scientific part for the PGE01-02-03. SAFNWC software version V1.0 released in 2004. Météo France.

Mallat S. G. and Hwang W. L., 1992. Singularity Detection And Processing With Wavelets. *IEEE Transactions on Information Theory*, 38: 617 – 643.

Morille Y., Haeffelin M., Drobinski P. and al., 2005, STRAT: Structure of the atmosphere from single channel LIDAR data, Submitted to Journal of Atmospheric and Oceanic Technology

Measures Raymond M., 1992, "*Laser Remote Sensing: Fundamentals and Applications*", Krieger Pub. Co.

Menzel W.P., Smith W.L. and Stewart T.R., 1983, Improved cloud motion wind vector and altitude assignement using VAS, Journal of Climate and Applied Meteorology, 22, 377-384.

Schmetz J., Hollmund K., Hoffman J. and B. Strauss, 1993, Operational cloud motion winds from Meteosat infrared images, Journal of Applied Meteorology, 32, 1207-1225.

SMHI, 2003. Scientific user manual for the AVHRR/AMSU cloud and precipitation products of the SAFNWC/PPS.

List of acronyms

AVHRR Advanced Very High Resolution Radiometer

BALTEX Baltic Sea Experiment

BBC Baltex Bridge Campaign

CLIWANET Cloud Liquid Water Network

CM SAFNWC Cloud Mask product

CM-SAF SAF on Climate Monitoring

CNN CLIWA-NET Network campaign

CT SAFNWC Cloud Type product

CTH Cloud Top Height

CTP Cloud Top Pressure

CTT Cloud Top Temperature

CTTH SAFNWC Cloud Top Temperature and Height product

DIAL Differential Absorption LIDAR

EU European Union

EUMETSAT European organization for the Exploitation of Meteorological Satellites

HIRLAM High Resolution Limited Area Model

IR Infrared

KNMI Royal Netherlands Meteorological Institute

LIDAR Light Detection And Ranging

LNA LIDAR Nuages Aerosols

METEOSAT Meteorological Satellite

MSG METEOSAT Second Generation

NOAA National Oceanic and Atmospheric Administration

NSPR No Significant Power Return

NWP	Numerical Weather Prediction model
PPS	Polar Platform System
RTM	Radiative Transfer Model
SAF	Satellite Application Facility
SAFNWC	SAF for support to Nowcasting and very short range forecasting
SEVIRI	Spinning Enhanced Visual and Infrared Imager
SIRTA	Site Instrumental de Recherche par Télédétection Atmosphérique
SMHI	Swedish Meteorological and Hydrological Institute
STRAT	Structure of the Atmosphere algorithm
UV	Ultraviolet

81 Alexandersson, H., Karlström, C., Larsson-McCann, S. (1991)
Temperaturen och nederbörden i Sverige 1961-90. Referensnormaler.

82 Vedin, H., Alexandersson, H., Persson, M. (1991)
Utnyttjande av persistens i temperatur och nederbörd för vårflödesprognoser.

83 Moberg, A. (1992)
Lufttemperaturen i Stockholm 1756 - 1990. Historik, inhomogeniteter och urbaniseringseffekt.
Naturgeografiska Institutionen, Stockholms Universitet.

84 Josefsson, W. (1993)
Normalvärden för perioden 1961-90 av globalstrålning och solskenstid i Sverige.

85 Laurin, S., Alexandersson, H. (1994)
Några huvuddrag i det svenska temperatur-klimatet 1961 - 1990.

86 Fredriksson, U. och Ståhl, S. (1994)
En jämförelse mellan automatiska och manuella fältmätningar av temperatur och nederbörd.

87 Alexandersson, H., Eggertsson Karlström, C. och Laurin S. (1997).
Några huvuddrag i det svenska nederbördsklimatet 1961-1990.

88 Mattsson, J., Rummukainen, M. (1998)
Växthuseffekten och klimatet i Norden - en översikt.

89 Kindbom, K., Sjöberg, K., Munthe, J., Peterson, K. (IVL)
Persson, C. Roos, E., Bergström, R. (SMHI). (1998)
Nationell miljöövervakning av luft- och nederbördskemi 1996.

90 Foltescu, V.L., Häggmark, L (1998)
Jämförelse mellan observationer och fält med griddad klimatologisk information.

91 Hultgren, P., Dybbroe, A., Karlsson, K.-G. (1999)
SCANDIA – its accuracy in classifying LOW CLOUDS

92 Hyvarinen, O., Karlsson, K.-G., Dybbroe, A. (1999)
Investigations of NOAA AVHRR/3 1.6 μm imagery for snow, cloud and sunglint discrimination
(Nowcasting SAF)

93 Bennartz, R., Thoss, A., Dybbroe, A. and Michelson, D. B. (1999)
Precipitation Analysis from AMSU
(Nowcasting SAF)

94 Appelqvist, Peter och Anders Karlsson (1999)
Nationell emissionsdatabas för utsläpp till luft - Förstudie.

95 Persson, Ch., Robertson L. (SMHI)
Thaning, L (LFOA). (2000)
Model for Simulation of Air and Ground Contamination Associated with Nuclear Weapons. An Emergency Preparedness Model.

96 Kindbom K., Svensson A., Sjöberg K., (IVL) Persson C., (SMHI) (2001)
Nationell miljöövervakning av luft- och nederbördskemi 1997, 1998 och 1999.

97 Diamandi, A., Dybbroe, A. (2001)
Nowcasting SAF
Validation of AVHRR cloud products.

98 Foltescu V. L., Persson Ch. (2001)
Beräkningar av moln- och dimdeposition i Sverigemodellen - Resultat för 1997 och 1998.

99 Alexandersson, H. och Eggertsson Karlström, C (2001)
Temperaturen och nederbörden i Sverige 1961-1990. Referensnormaler - utgåva 2.

100 Korpela, A., Dybbroe, A., Thoss, A. (2001)
Nowcasting SAF - Retrieving Cloud Top Temperature and Height in Semi-transparent and Fractional Cloudiness using AVHRR.

101 Josefsson, W. (1989)
Computed global radiation using interpolated, gridded cloudiness from the MESA-BETA analysis compared to measured global radiation.

102 Foltescu, V., Gidhagen, L., Omstedt, G. (2001)
Nomogram för uppskattning av halter av PM_{10} och NO_2

103 Omstedt, G., Gidhagen, L., Langner, J. (2002)
Spridning av förbränningsemissioner från småskalig biobränsleeldning
– analys av PM2.5 data från Lycksele med hjälp av två Gaussiska spridningsmodeller.

104 Alexandersson, H. (2002)
Temperatur och nederbörd i Sverige 1860 - 2001

105 Persson, Ch. (2002)
Kvaliteten hos nederbördskemiska mätdata som utnyttjas för dataassimilation i MATCH-Sverige modellen".

106 Mattsson, J., Karlsson, K-G. (2002)
CM-SAF cloud products feasibility study in the inner Arctic region
Part I: Cloud mask studies during the 2001 Oden Arctic expedition

107 Kärner, O., Karlsson, K-G. (2003)
Climate Monitoring SAF - Cloud products feasibility study in the inner Arctic region.
Part II: Evaluation of the variability in radiation and cloud data

108 Persson, Ch., Magnusson, M. (2003)
Kvaliteten i uppmätta nederbördsmängder inom svenska nederbörskemiska stationsnät

109 Omstedt, G., Persson Ch., Skagerström, M (2003)
Vedeldning i småhusområden

110 Alexandersson, H., Vedin, H. (2003)
Dimensionerande regn för mycket små avrinningsområden

111 Alexandersson, H. (2003)
Korrektion av nederbörd enligt enkel klimatologisk metodik

112 Joro, S., Dybbroe, A.(2004)
Nowcasting SAF – IOP
Validating the AVHRR Cloud Top Temperature and Height product using weather radar data
Visiting Scientist report

113 Persson, Ch., Ressner, E., Klein, T. (2004)
Nationell miljöövervakning – MATCH-Sverige modellen
Metod- och resultatsammanställning för åren 1999-2002 samt diskussion av osäkerheter, trender och miljömål

114 Josefsson, W. (2004)
UV-radiation measured in Norrköping 1983-2003.

115 Martin, Judit, 2004
Var tredje timme – Livet som väderobservatör

116 Gidhagen, L., Johansson, C., Törnquist, L. (2004)
NORDIC – A database for evaluation of dispersion models on the local, urban and regional scale

117 Langner, J., Bergström, R., Klein, T., Skagerström, M. (2004)
Nuläge och scenarier för inverkan på marknära ozon av emissioner från Västra Götalands län – Beräkningar för 1999